

A study on the diffusion-induced grain boundary migration ahead of stress corrosion cracking crack tips through advanced characterization

Zhao Shen^{a,*}, Koji Arioka^b, Sergio Lozano-Perez^a

^aDepartment of Materials, University of Oxford, Parks Road, OX1 3PH Oxford, UK

^bInstitute of Nuclear Safety Systems, Inc. (INSS), 64 Sata, Mihama-cho, Mikata-gun, Fuku, Mihama 919-1205, Japan

Corresponding author: zhao.shen@materials.ox.ac.uk

Abstract: Three austenitic alloys with different Ni content were stress corrosion cracking (SCC) tested in simulated pressurized water reactor (PWR) primary water at 320 and 360°C. Diffusion-induced grain boundary migration (DIGM) associated with preferential intergranular oxidation (PIO) is observed ahead of all SCC crack tips. The occurrence of DIGM is revealed to be driven by PIO-induced diffusion of Cr, Fe, and Ni. The extent of DIGM is controlled by the lateral and in-depth elemental diffusion and PIO, with these processes interconnected. Temperature and alloy composition are revealed to affect the extent of DIGM by affecting these processes.

Key words: Austenitic alloy; Stress corrosion cracking; Diffusion-induced grain boundary migration; Chemical diffusion; Transmission electron microscopy.

1. Introduction

The different behaviours of grain boundaries (GBs) in metals have attracted a great deal of interest for many decades since many useful properties of metals are, to some extent, controlled by GBs [1, 2]. Among these behaviours, grain boundary migration (GBM), defined as the movement of a GB in a direction perpendicular to the tangent plane of the boundary, has been most extensively studied [2-12]. According to the work presented in the literature, the driving forces behind the GBM can be mainly divided into two types: atom diffusion and stress, corresponding to diffusion-induced GBM (DIGM) [2-8] and stress-driven GBM [9-12], respectively. Balluffi and Cahn [4] reported that the controlling mechanism of the DIGM is the unequal diffusion of solute and solvent atoms. Rupert et al. [12] experimentally observed that the shear stress can directly cause the GBs to move and is believed to be the controlling mechanism of stress-driven GBM.

Stress corrosion cracking (SCC) is one of the most common degradation phenomena in the structural materials, mainly austenitic alloys, within pressurized water reactors (PWRs) [13, 14]. SCC-induced failures have been frequently reported in these structural materials during the long-term operation in PWR primary water environment [15, 16]. These failures have led to substantial economic losses from service outages and costs for replacement components. For this reason, a mechanistic understanding of SCC is required in order to mitigate the SCC-related failures and better predict the service lifetime of the structural materials. A great research effort on SCC has been paid by the nuclear industry in the past decades. Although a number of factors have been revealed to be able to affect the process of SCC [17-26], the controlling mechanisms are still under debate. Among the most relevant ones, including the film-rupture model [27, 28], the hydrogen embrittlement model [29, 30], the creep-cavity model [31, 32], and the preferential intergranular oxidation (PIO) model [20, 33-39]. Among these models, the PIO model is the one that seems to describe the degradation in PWR primary water most realistically. According to the PIO model, there is a strong correlation between the SCC properties and the microstructure and microchemistry around the SCC crack tips. In addition, the mechanism suggests that the factors that can affect intergranular oxidation ahead of the SCC crack tip then they can also influence SCC crack growth.

With the recent substantial improvement of high-resolution characterization techniques, such as atom probe tomography (APT), transmission electron microscopy (TEM), and transmission Kikuchi diffraction (TKD), more details around the SCC crack tips can now be observed [33-41]. Among these observations, a Ni-rich zone has been frequently observed ahead of the SCC crack tips after exposure to PWR primary water [17, 19, 21, 22, 25, 33, 34, 37-41]. At the early stages, the Ni-rich zone formed under the PWR primary water environment is small and its formation mechanisms and effects on SCC have been scarcely studied. Since the SCC of Alloy 600 in hydrogenated steam at temperatures above 400 °C was shown to share the same mechanism with 320 °C PWR primary water by Economy et al. [42], the high-temperature hydrogenated steam is assumed to replicate the electrochemical conditions of the PWR primary water. Recently, low-pressure hydrogenated steam has been used as an accelerated environment to simulate the intergranular oxidation occurred in the PWR primary water and the Ni-rich zone was also observed [39, 43-47]. Due to the increase of temperature in the hydrogenated steam (480 °C vs. 320 °C), the size of the Ni-rich zone was much greater than that observed in the PWR primary water [17, 19, 21, 25, 33, 34, 37-41, 49, 50]. After that, GBM started to be frequently reported in the Ni-based alloys after exposure to simulated PWR primary water [21, 22, 34, 38, 39, 41, 43-53].

The GBM zone observed in the austenitic alloys after exposure to the high-temperature hydrogenated steam and the PWR primary water has always been observed to be depleted in Cr and Fe and enriched in Ni. This is similar to the results reported in [4] where the process of GBM is revealed to be driven by the solute elements diffusion. Considering the similarities between the GBM reported by the SCC community and in [4], it is also termed as DIGM by the SCC community [20, 22, 35, 41, 43-49]. To date, a lot of studies about the potential roles of DIGM in SCC have been conducted, while they are mainly focused on how DIGM affects intergranular oxidation rate [43-49]. Intergranular oxides ahead of the crack tips have been reported to be porous [17, 34, 38] and micro-mechanical testing conducted by Dohr et al. [26] showed that 350-575 MPa of stress is still needed to break the oxidized GBs. Therefore, to activate SCC crack propagation, a certain amount of stress is required to break the intergranular oxides or the crack may not grow no matter how fast the intergranular oxidation rate is. As a result, a greater intergranular oxidation rate may not necessarily result in a faster SCC crack growth rate (CGR). Compared with the intergranular oxidation rate, CGR is a more important parameter to the mechanistic understanding of SCC and to the industry. To obtain a more direct understanding of the relationship between DIGM and SCC crack propagation, it is essential to make experimental observations of DIGM around the active SCC crack tips. In addition, although the occurrence of DIGM at the oxidized GBs is believed to be driven by the diffusion of solute elements, a detailed mechanistic study on the DIGM occurring ahead of SCC crack tips is still missing, which may shed light on the understanding of the effects of DIGM on the SCC crack growth.

To date, the study of DIGM has mainly focused on Ni-based austenitic alloys, such as Alloy 600 [20, 22, 34, 35, 38, 43-48, 51] and Alloy 690 [39, 41, 54]. Recent work conducted by Meisnar et al. [53] and Shen et al. [55, 56] also found DIGM

in 316 stainless steel, which is a widely used Fe-based austenitic alloy in the nuclear industry. In order to improve our understanding of DIGM in austenitic alloys (Fe- and Ni-based) under the PWR primary water conditions and its role on SCC, a more comprehensive study is needed.

In this study, 3 austenitic alloys with similar Cr and different Ni content (Fe-16Cr-xNi) were SCC tested in simulated PWR primary water at 320 and 360 °C. After the SCC tests, advanced characterization techniques were combined to conduct detailed examinations around the SCC crack tips. With the high-resolution results, new insights into the DIGM occurring ahead of the SCC crack tips can be acquired. In addition, a new method was proposed to quantify the DIGM ahead of the SCC crack tips, providing a better understanding of the effect of DIGM on SCC crack growth.

2. Experimental

2.1 Materials and SCC tests

The materials used in this study are Fe-16Cr-11Ni alloy, Fe-16Cr-60Ni alloy, and Fe-16Cr-75Ni (Alloy 600) alloy after SCC tests under PWR primary water (500 ppm B + 2 ppm Li + 30 cc/kg dissolved H₂) at 320 and 360 °C. These alloys were part of a much wider study commissioned in Japan and were made available for this work [57]. The alloy composition of these materials is listed in Table 1. The average grain sizes for Fe-16Cr-11Ni alloy, Fe-16Cr-60Ni alloy, and Fe-16Cr-75Ni alloy are around 90 µm, 300 µm, and 120 µm, respectively. There were 20-30% of intergranular carbides were observed in Fe-16Cr-60Ni alloy while they were not observed in Fe-16Cr-11Ni alloy and Fe-16Cr-75Ni alloy. Cold work (CW) in austenitic alloys was shown to increase SCC susceptibility while it is inevitable during manufacturing and installation [58–62]. As a result, to take into account of the effects of CW on SCC, all of the materials used in this study were cold-worked. CW in the specimens was produced through uni-directional rolling at room temperature to a thickness reduction of 20%.

Table 1 Chemical composition of the materials used in this study (wt. %)

Materials	C	Cr	Fe	Si	Mn	P	S	Ni	Mo	Cu
Fe-16Cr-11Ni alloy	0.047	16.45	68.54	0.45	1.42	0.024	0.001	11.00	2.07	-
Fe-16Cr-60Ni alloy	0.026	16.17	23.05	0.28	0.41	0.002	0.001	60.06	-	-
Fe-16Cr-75Ni alloy	0.06	16.02	6.94	0.33	0.35	0.006	0.001	75.26	-	0.03

Table 2 Three alloys bulk specimen data: test temperature; calculated CGR; number of SCC crack tips analysed.

Materials	Temperature (°C)	CGR (mm/s)	Crack tips analyzed
Fe-16Cr-11Ni alloy	320	1.8×10^{-7}	3
	360	1.6×10^{-7}	3
Fe-16Cr-60Ni alloy	320	7.1×10^{-7}	3
	360	8.4×10^{-8}	3
Fe-16Cr-75Ni alloy	320	9.3×10^{-7}	3
	360	4.8×10^{-6}	2

The SCC tests were conducted by INSS (Japan) using pre-cracked 0.5T compact tension (CT) specimens in an autoclave under a constant stress intensity factor of 30 MPa m^{1/2}. The crack growth direction for these alloys was in T-L orientation which is parallel to the cold-rolling direction. More details can be found in [57]. The CGRs for Fe-16Cr-11Ni alloy, Fe-16Cr-60Ni alloy, and Fe-16Cr-75Ni alloy at different temperatures are obtained by measuring the crack lengths on the fracture surface and the related test durations. The measured CGRs and the number of crack tips for each alloy are listed in Table 2. To minimize the potential effects of GB character, all the crack tips in this study were prepared from high-angle GBs. In addition, to remove the potential effect of intergranular carbides on the intergranular oxidation and DIGM, the crack tips in Fe-16Cr-60Ni alloy were prepared from the region where was free of intergranular carbides. Since the microstructure and microchemistry around the SCC crack tips could be affected by the exposure time, to minimise the differences caused by the exposure time, the SCC crack tips were prepared from the SCC crack front. As a result, all the crack tips are assumed to be potentially active. Although the crack tips used in the present study are potentially active, the different CGRs of these alloys under different temperature may also affect the exposure times of these crack tips. Since the SCC cracks are very tight, bright-field TEM (BFTEM) imaging and high-angle annular dark-field (HAADF) imaging were combined to identify the location of SCC crack tips. More details about this approach can be found in [38].

2.2 Characterization techniques

The site-specific TEM foils used in this study were prepared by a dual beam Zeiss NVision 40 FIB-SEM with a thickness of about 50 nm. A JEOL 2100 TEM operating at 200 kV was used to perform imaging and selected area electron diffraction. A C_s aberration-corrected JEOL ARM200F TEM operating at 200 kV and equipped with a Quantum Gatan image filter (GIF) spectrometer was used for HAADF imaging and Electron Energy Loss Spectroscopy (EELS) chemical composition analysis. The convergence and collection half-angles were 31 and 41 mrad, respectively. EELS quantification was performed in Digital Micrograph by the background subtraction method. TKD analysis was performed on the TEM foils using a Zeiss Merlin SEM equipped with Bruker Optimus TKD Detector head that allows for better spatial resolution with minimal sample drift. The data was subsequently post-processed by Channel 5 software. More details can be found in [53].

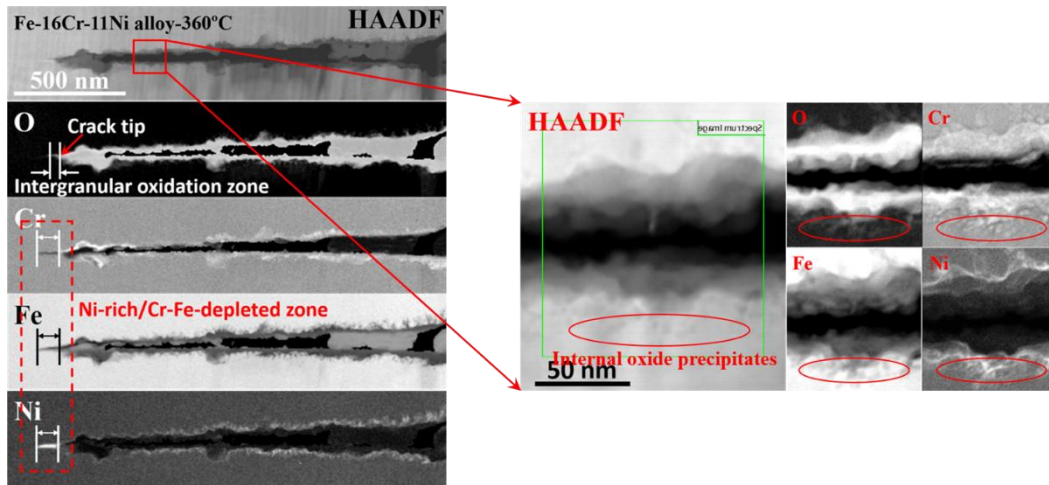
3. Results

Several potential precursors required for the SCC crack growth were identified in our previous work [22, 34, 38], including intergranular oxidation ahead of crack tips, defects accumulated around the crack tip, porous intergranular oxide, and DIGM. The following sections will mainly focus on how DIGM changes with alloy composition (Ni content) and temperature by using advanced characterization.

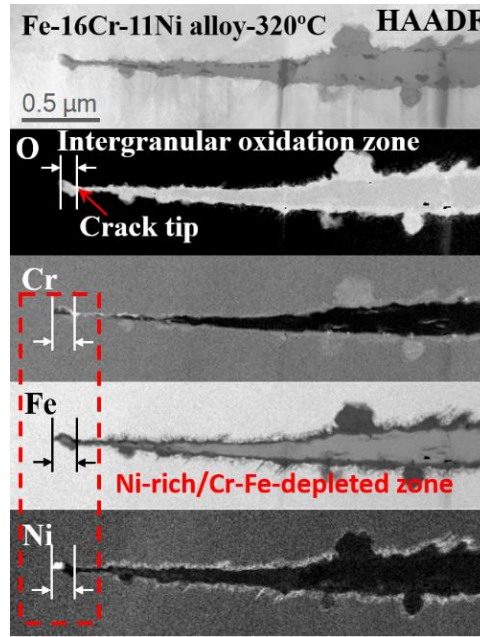
3.1 Morphology and elemental distribution of SCC cracks

3.1.1 Fe-16Cr-11Ni alloy

The morphology and elemental distribution of the SCC cracks were characterized by HAADF imaging and EELS analysis. One of the representative cracks prepared from Fe-16Cr-11Ni alloy tested at 360 °C is shown in Fig. 1a. It is seen that the oxidation has developed into the GB ahead of the crack tip, resulting in the formation of a Cr-rich intergranular oxidation zone (IOZ). The IOZ length is ~72 nm. In addition, a Cr-Fe depleted/Ni enriched zone is observed aside the IOZ. The length of this zone ahead of the SCC crack tip is measured to be ~165 nm. The HAADF image shows that the crack opening is mostly full of oxide. It is worth noting that the crack opening was full of oxide, and the FIB milling during sample preparation resulted in the exfoliation of a part of oxide from the crack opening. The qualitative EELS elemental maps, in which the brighter region contains a greater net count of atoms, show that the oxides in the crack opening are Fe-rich (see Fig. 1a). The atomic ratio of the oxide particles in the crack opening shows that they are very likely Fe₃O₄, which is consistent to the results reported in the literature [56]. The magnified image shows that the crack flanks have also been oxidized. The oxides on the crack flanks are mainly composed of Cr and Fe, which has been reported to be Cr-Fe spinel [55, 56]. Ni is nearly exhausted in the oxides and is believed to be expelled to the surrounding regions. Due to the increased resolution, discrete oxide precipitates and Ni segregation surrounding these precipitates are observed under the Cr-Fe spinel oxide layer. The formation of the discrete Cr-rich oxide precipitates has been proven to be due to low-temperature internal oxidation [55]. Similar results about the Ni segregation have also been reported by Shen et al. [56] in the study of 316 stainless steel exposed to PWR primary water at 340 °C via TEM and by Kruska et al. [63] in the study of 304 stainless steel exposed to PWR primary water at 360 °C via APT. Further observation shows that the thickness of the Cr-Fe spinel oxide layer on the crack flanks is not uniform, decreasing in the direction towards the crack tip from ~50 nm to less than 10 nm. The different thicknesses at different regions can be attributed to the different exposure times to the PWR primary water as the crack kept growing during the test.



(a)



(b)

Fig. 1. HAADF images and qualitative EELS elemental maps of representative SCC crack tips prepared from Fe-16Cr-11Ni alloy tested at (a) 360 °C and (b) 320 °C.

Fig. 1b shows the morphology and elemental distribution of a representative SCC crack prepared from Fe-16Cr-11Ni alloy tested at 320 °C. Both the morphology and elemental distribution observed in this crack are very similar to that observed in the crack tested at 360 °C. Intergranular oxidation has developed into the region ahead of the SCC crack tip, forming an IOZ with a length of ~115 nm. A Cr-Fe depleted/Ni enriched zone is also observed, with a length of ~170 nm. The crack opening is full of Fe-rich oxide and crack flank oxidation is also observed. A Cr-Fe spinel oxide layer is observed on the crack flanks. Discrete Cr-rich oxide precipitates and Ni segregation are also observed at the interface between the Cr-Fe spinel oxide layer and the metal matrix.

3.1.2 Fe-16Cr-60Ni alloy

Fig. 2a shows the morphology and elemental distribution of a representative SCC crack prepared from Fe-16Cr-60Ni alloy tested at 360 °C. It is seen that the intergranular oxidation has developed into the region ahead of the SCC crack tip, forming an IOZ with a length of ~1250 nm. A Cr-Fe depleted/Ni enriched zone is also observed aside the IOZ. The length of this zone is measured to be ~1850 nm. Further observation on the HAADF image shows that the crack morphology is very different from that observed in the Fe-16Cr-11Ni alloy. The crack appears to have a tortuous shape. In addition, the crack opening is much tighter than that observed in the Fe-based austenitic alloys. The curved shape of the crack is very similar to the oxidized GBs of Alloy 600 after exposure to hydrogenated steam at 480 °C [43-45, 47, 48]. These authors attributed the formation of the curved GBs to the DIGM. Compared with the Fe-rich oxide in the crack opening of the Fe-16Cr-11Ni alloy, the oxide in the crack opening of the Fe-16Cr-60Ni alloy is enriched in Cr, which is also very similar to the results observed in the oxidized GBs of the Alloy 600 in hydrogenated steam at 480 °C [43-45, 47, 48]. Due to the tight crack opening, it is difficult to differentiate the oxide formed on the crack flanks from the oxide in the crack opening. As shown in the magnified HAADF image and EELS elemental maps (Fig. 2a), discrete Cr-rich oxide precipitates and Ni segregation surrounding these precipitates are not observed in neither of the crack flanks.

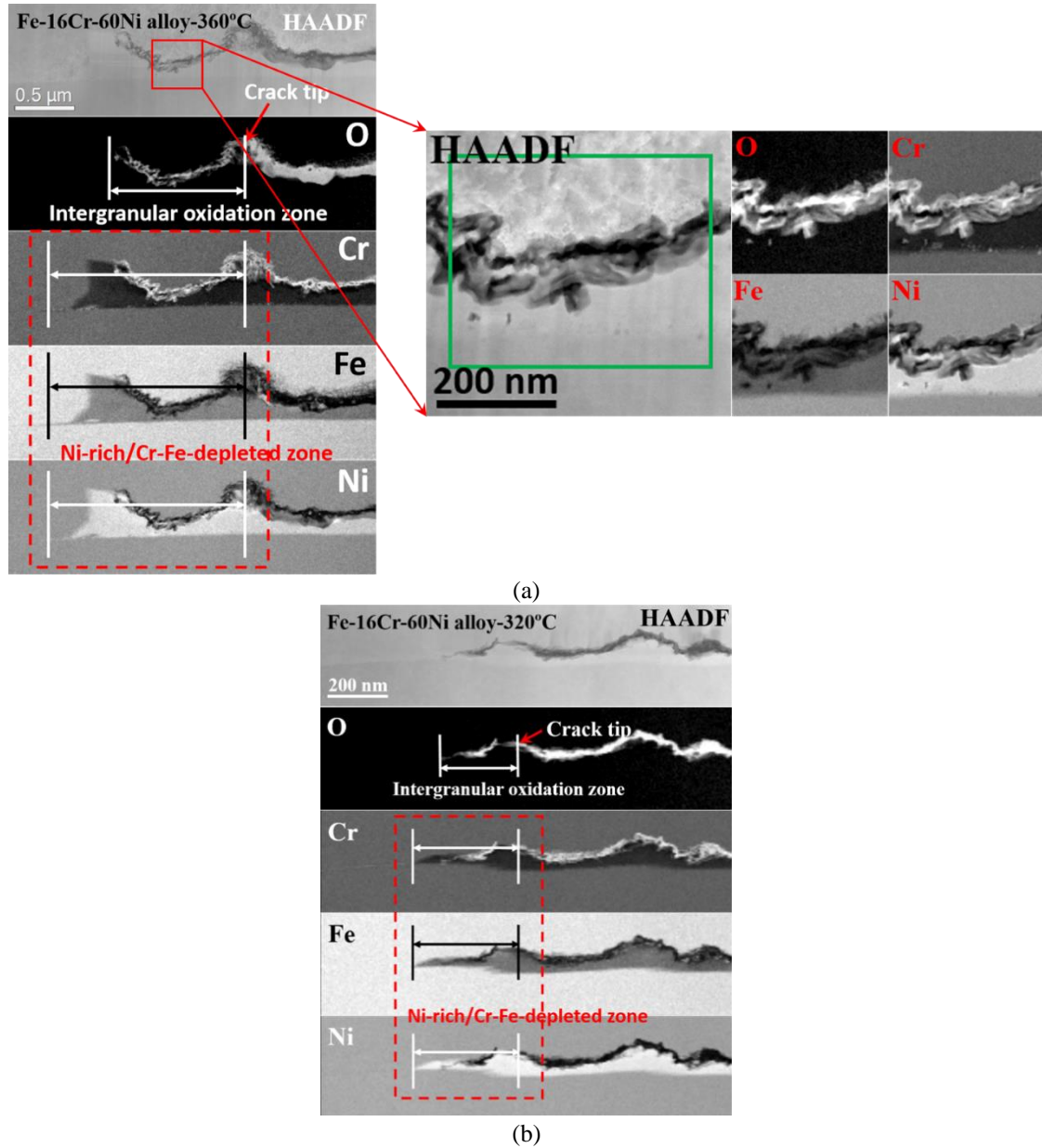


Fig. 2. HAADF images and qualitative EELS elemental maps of representative SCC crack tips prepared from Fe-16Cr-60Ni alloy tested at (a) 360 °C and (b) 320 °C.

Fig. 2b shows the morphology and elemental distribution of a representative SCC crack prepared from Fe-16Cr-60Ni alloy tested at 320 °C. Both the morphology and elemental distribution of the crack are similar to the crack prepared from Fe-16Cr-60Ni alloy tested at 360 °C. An IOZ is observed ahead of the SCC crack tip, with a length of ~260 nm. A Cr-Fe depleted/Ni enriched zone is also observed aside the IOZ, with a length of ~340 nm. The crack shape is tortuous and the crack opening is very tight. Discrete Cr-rich oxide precipitates and Ni segregation surrounding these precipitates are observed in neither of the crack flanks.

3.1.3 Fe-16Cr-75Ni alloy

Fig. 3a shows the morphology and elemental distribution of a representative SCC crack prepared from Fe-16Cr-75Ni alloy tested at 360 °C. This crack has been reported in [34]. Both an IOZ and a Cr-Fe depleted/Ni enriched zone are observed ahead of the SCC crack tip, with the lengths of ~360 nm and ~725 nm, respectively. Similarly to the Fe-16Cr-60Ni alloy, the SCC crack in Fe-16Cr-75Ni alloy tested at 360 °C also has a tortuous shape. In addition, the crack opening is very tight and the oxide in the crack opening is also enriched in Cr. Discrete Cr-rich oxide precipitates and Ni segregation surrounding these precipitates are not observed in both crack flanks. Fig. 3b shows the morphology and elemental distribution of a representative SCC crack prepared from Fe-16Cr-75Ni alloy tested at 320 °C. Both an IOZ and a Cr-Fe depleted/Ni enriched zone are observed ahead of the SCC crack tip. The lengths of the IOZ and Ni-rich zone are ~90 nm and ~175 nm,

respectively. The crack opening is narrow and also full of Cr-rich oxide. Discrete Cr-rich oxide precipitates and Ni segregation surrounding these precipitates are also not observed.

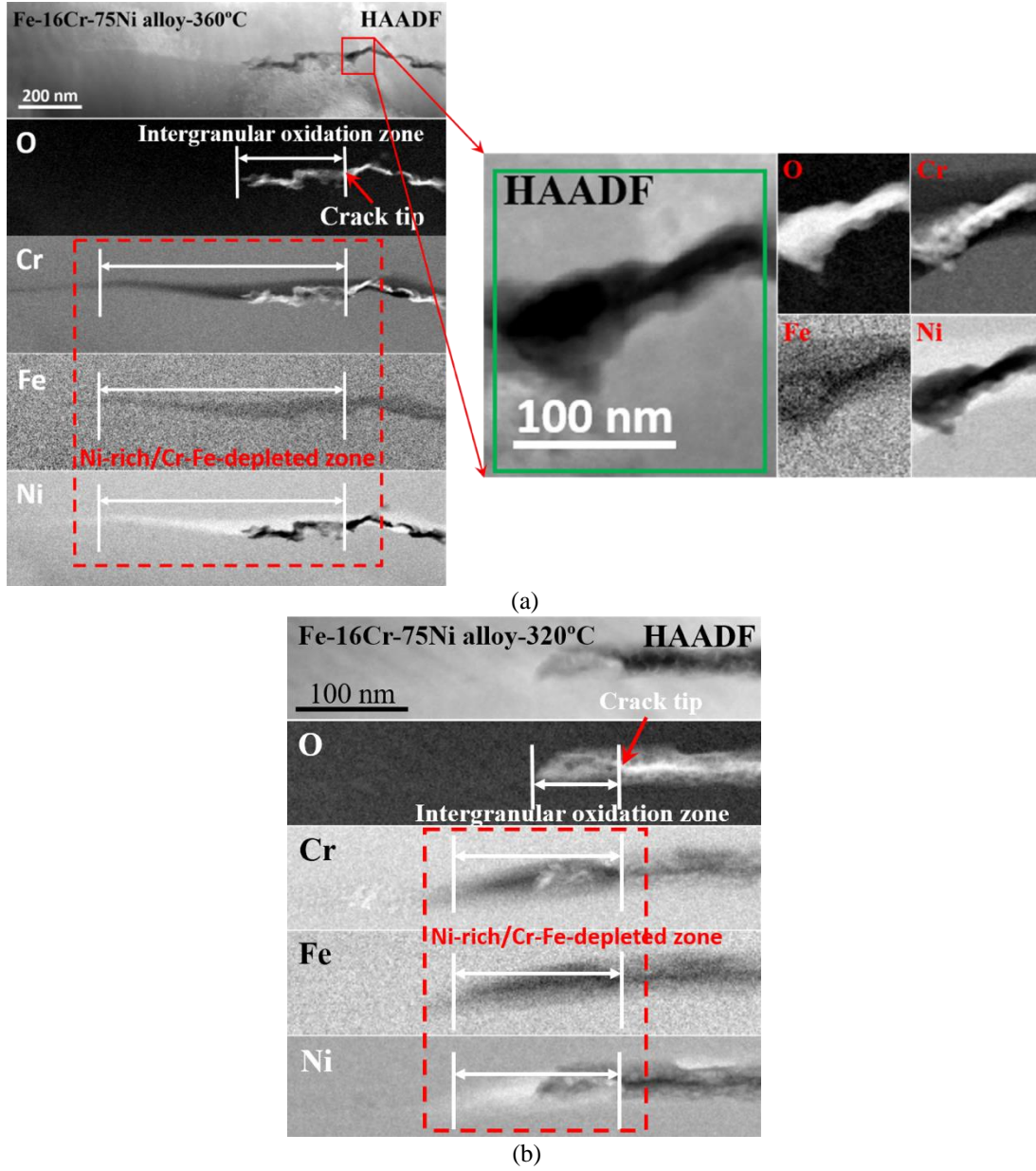


Fig. 3. HAADF images and qualitative EELS elemental maps of representative SCC crack tips prepared from Fe-16Cr-76Ni alloy tested at (a) 360 °C [34] and (b) 320 °C.

3.2 High-resolution analytical characterization of DIGM ahead of SCC crack tips

The Cr-Fe depleted/Ni enriched zone has been frequently reported in the study of GB oxidation [43-51, 63-66] and SCC crack tips [19, 21, 22, 25, 34, 37, 38, 40, 41, 52, 53, 55, 56]. Due to the improvement of the characterization resolution, the Ni-rich zone has been associated with DIGM [22, 34, 38, 41, 43, 44, 46-51, 55, 56, 66]. The Ni-rich zone has been observed ahead of all crack tips examined in the present study. Depending on the size of the Ni-rich zone ahead of the SCC crack tips, TKD [22], selective area electron diffraction (SAED) [43] or atomic-resolution imaging [41] were applied to examine the crystallographic orientation relationship between the Ni-rich zone and the surrounding metal matrix. The results confirm that all the Ni-rich zones ahead of the SCC crack tips are formed due to DIGM. The formation of DIGM ahead of SCC crack tips has been generally believed to be due to the selective oxidation of Cr and Fe. In order to achieve a better understanding of the formation mechanism, a higher resolution analytical characterization was conducted around the SCC crack tips, as shown below. In this section, the representative crack tips tested at 360 °C are selected as examples to study the DIGM around the SCC crack tips in the three different alloys.

3.2.1 Fe-16Cr-11Ni alloy

A HAADF image of a representative crack tip prepared from Fe-16Cr-11Ni alloy tested at 360 °C is shown in Fig. 4a. Since the atomic densities of oxide and metal matrix are different, these two phases can be easily differentiated according to the HAADF image contrast. Fig. 4b shows the qualitative EELS elemental maps, in which a brighter signal represents a higher number of atoms in projection. A Ni-rich zone formed by DIGM is observed ahead of the crack tip. The positions of the original and migrated GBs are marked by the red and blue dashed lines, respectively. The intergranular oxidation ahead of the crack tip propagates along the migrated GB instead of the original GB. A quantitative EELS line-scan was conducted to reveal the chemical composition across the DIGM zone and IOZ. Fig. 4c shows that the migrated zone is enriched in Ni and depleted in Cr and Fe while the IOZ is enriched Cr and depleted in Ni and Fe. Due to the small volumes of the IOZ and the DIGM zone, signal overlap between them is likely to have occurred (Fig. 4c). Hence, the chemical compositions measured from the IOZ and the DIGM zone are not accurate. Compared with TEM, APT offers a truly 3D analysis and a higher analytical spatial resolution [40, 49, 50, 66-68]. In a recent study conducted by Meisnar et al. [40], APT was employed to study the intergranular oxidation and DIGM ahead of the SCC crack tip in the Fe-16Cr-11Ni alloy tested at 360 °C. The atomic ratio of the oxide in the IOZ show that it mainly consists of Cr-Fe-Ni spinel. The chemical composition in the DIGM zone was reported to be 55-60% Ni, 30-35% Fe, 1-5% Cr (in atomic percentage) [40].

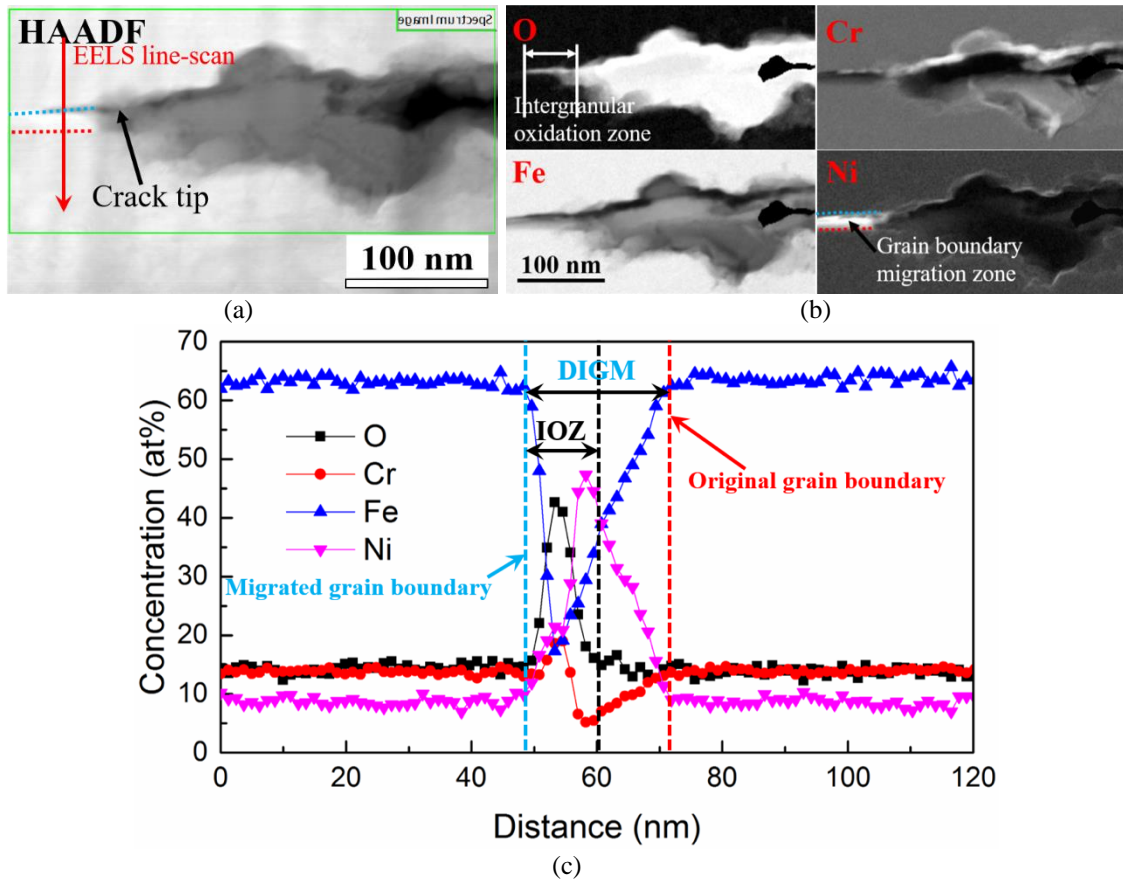


Fig. 4. (a) HAADF image showing the morphology around a representative crack tip prepared from Fe-16Cr-11Ni alloy tested at 360 °C; (b) EELS elemental O K edge and Cr/Fe/Ni L edge maps; (c) EELS quantitative composition line profiles across the IOZ and DIGM zone.

3.2.2 Fe-16Cr-60Ni alloy

Fig. 5a shows the high-resolution HAADF image of a representative SCC crack tip prepared from Fe-16Cr-60Ni alloy tested at 360 °C. Due to the big scale of the IOZ ahead of the crack tip, only the tip region of the IOZ is covered. The qualitative EELS elemental maps show that the DIGM also occurs and is associated with the formation of Cr-rich IOZ (Fig. 5b). The positions of the original and migrated GBs are marked by the red and blue dashed lines, respectively. Compared with the straight original GB, the migrated GB is very tortuous. Since the growth of the IOZ ahead of the crack tip develops along the migrated GB, the shape of the IOZ is also tortuous. A quantitative EELS line-scan was also conducted across the DIGM zone and IOZ. The results show that the oxides in the IOZ are enriched in Cr and depleted in Fe and Ni (Fig. 5c). The atomic ratio of the oxide in the IOZ show that it also mainly consists of Cr-Fe-Ni spinel. Due to a sharp edge between

the DIGM zone and the IOZ, there is nearly no overlap between these two regions, as shown in Fig. 5c. As a result, the chemical composition in the DIGM zone can be conveniently obtained from the EELS line profiles, which is 78-85% Ni, 10-13% Fe, 5-8% Cr (in atomic percentage). The chemical composition in the DIGM zone is not constant and a composition gradient is observed in the direction perpendicular to the GB plane (Fig. 5c).

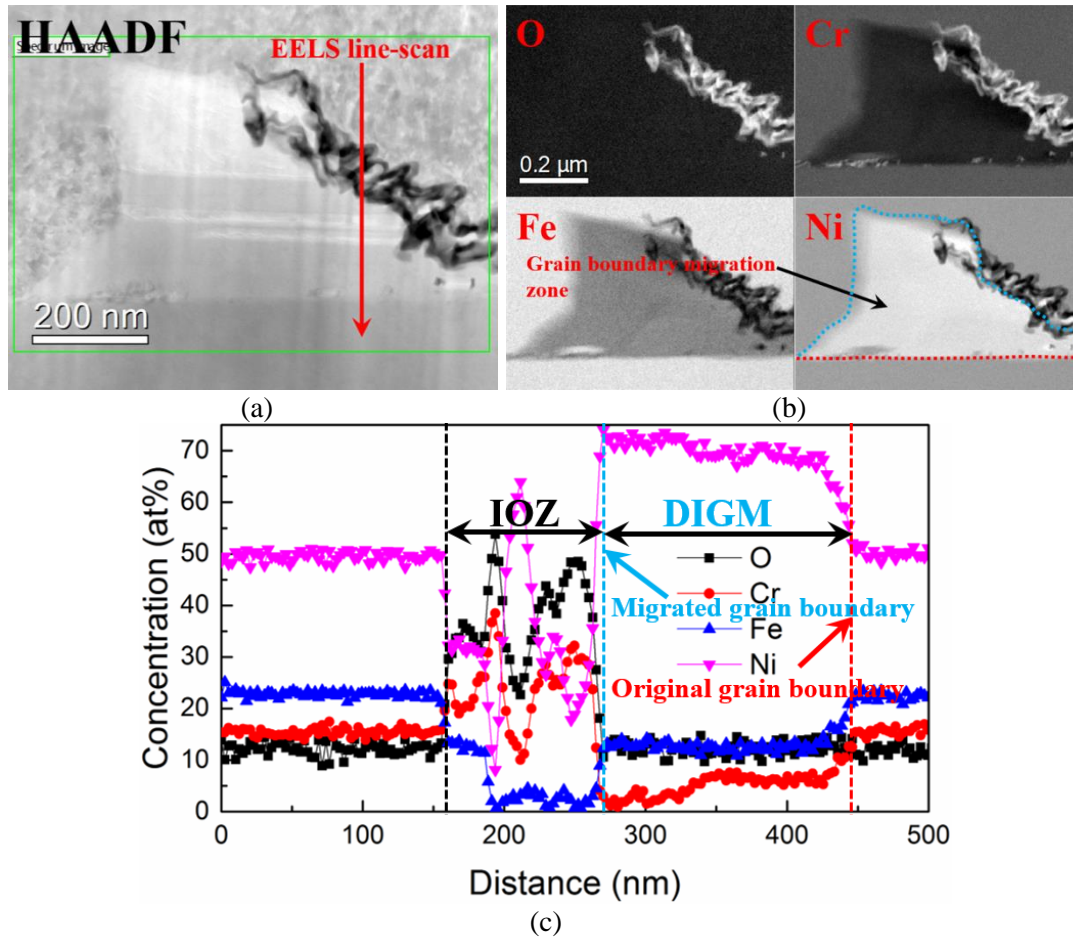
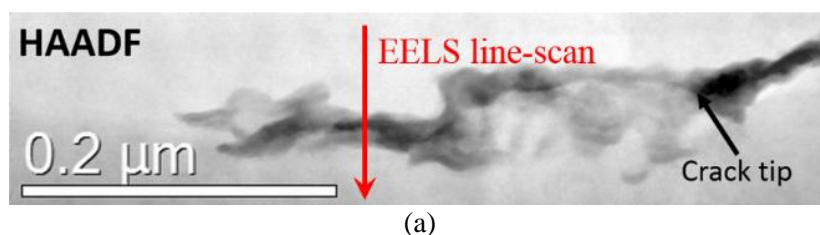


Fig. 5. (a) HAADF image showing the morphology around a representative crack tip prepared from Fe-16Cr-60Ni alloy tested at 360 °C; (b) EELS elemental O K edge and Cr/Fe/Ni L edge maps; (c) EELS quantitative composition line profiles across the IOZ and DIGM zone.

3.2.3 Fe-16Cr-75Ni alloy

Fig. 6a shows a HAADF image of a representative SCC crack tip prepared from Fe-16Cr-75Ni alloy tested at 360 °C. DIGM is also observed ahead of the crack tip. The positions of the original and migrated GBs are marked by the red and blue dashed lines, respectively (Fig. 6b). The oxidation has propagated into the migrated GB ahead of the crack tip, forming an IOZ. The IOZ is enriched in Cr and depleted in Fe and Ni. The atomic ratio of the oxide in the IOZ show that it mainly consists of Cr-Fe-Ni spinel. Ni is enriched in the DIGM zone and both Fe and Cr are depleted. Further observation reveals the existence of a composition gradient in the direction perpendicular to the GB plane. The concentrations of Cr and Fe decrease from the migrated GB outwards into the metal matrix while Ni shows an opposite trend. This chemical composition gradients could also be caused by a projection artefact, where the DIGM-matrix interface is not perpendicular to the TEM sample surface. The chemical composition in the GBM zone is 75-86%at. Ni, 2-7%at. Fe, 8-17%at. Cr (Fig. 6c).



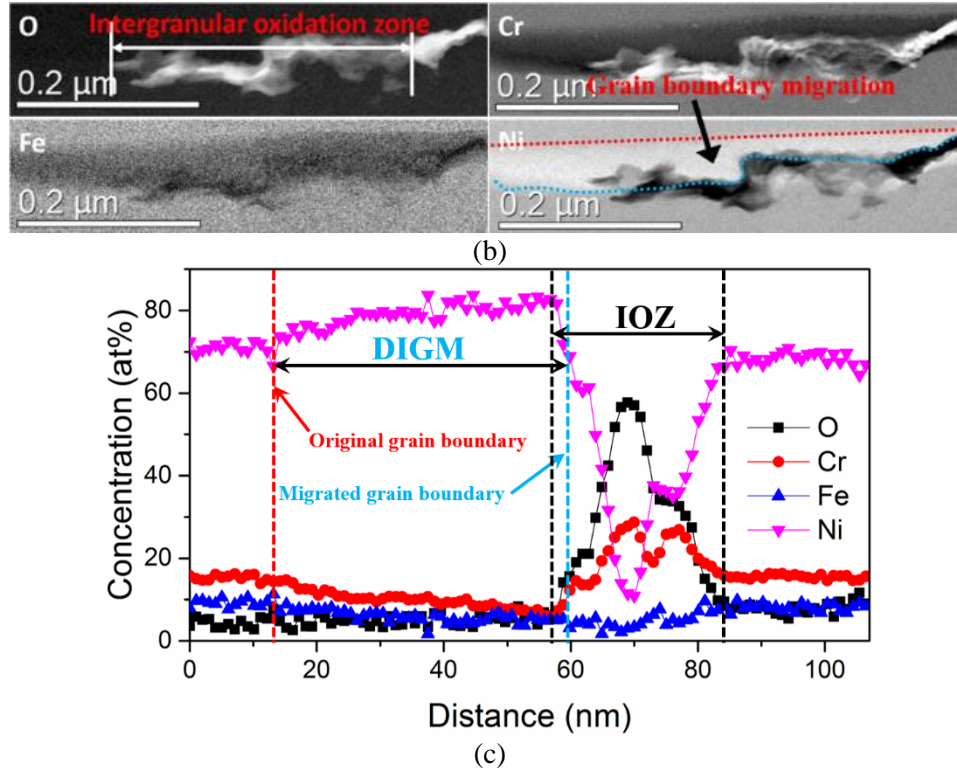


Fig. 6. (a) HAADF image showing the morphology around a representative crack tip prepared from Fe-16Cr-75Ni alloy tested at 360 °C; (b) EELS elemental O K edge and Cr/Fe/Ni L edge maps; (c) EELS quantitative composition line profiles across the IOZ and DIGM zone.

Table 3 Characterization data summarization for the three austenitic alloys tested at 320 and 360 °C: length of IOZ, length of DIGM zone, and maximum DIGM-induced deviation. The parameters displayed are calculated and averaged from all crack tips from a given alloy and a given temperature.

Materials	Temperature (°C)	IOZ length (nm)	DIGM zone length (nm)	Maximum DIGM deviation (nm)
Fe-16Cr-11Ni alloy	320	95±27	189±37	32±15
	360	87±24	196±44	38±12
Fe-16Cr-60Ni alloy	320	225±35	262±37	101±26
	360	1150±245	1625±225	525±62
Fe-16Cr-75Ni alloy	320	132±40	262±47	43±15
	360	343±46	505±220	81±23

According to the results presented above, once the DIGM occurs, both the intergranular oxidation and crack propagation will develop along the migrated GBs. In a recent work conducted by the authors [22], it is reported that the DIGM-induced deviation from the straight original GBs to the tortuous migrated GBs will decrease the effective stress loaded at the crack tips during the process of SCC crack propagation, resulting in a slower CGR. Since the DIGM-induced deviation in a specific GB is not uniform, the maximum deviation caused by the DIGM is used to quantify the effect of DIGM on the decrease of effective stress at the SCC crack tips. It is believed that a greater DIGM-induced GB deviation leads to a greater decrease of effective stress at the SCC crack tip, resulting in a slower CGR. The method used to measure the maximum DIGM-induced GB deviation is schematically shown in Fig. 7.

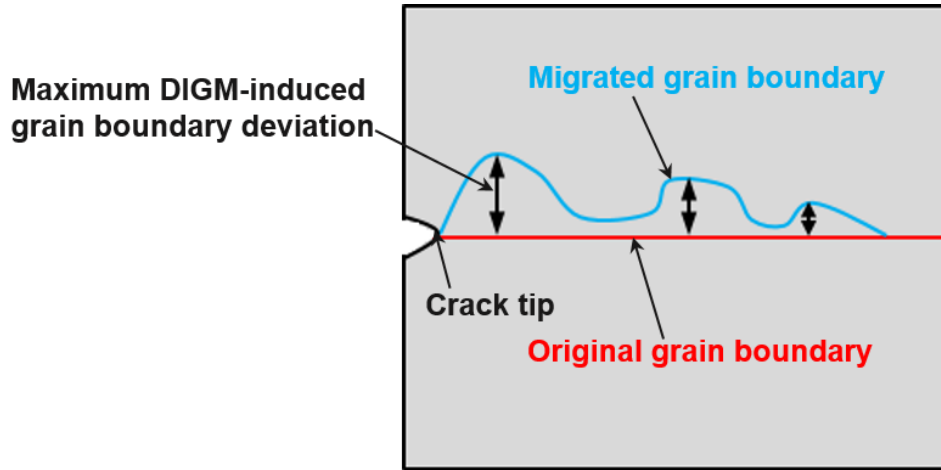


Fig. 7. Schematic illustration of DIGM-induced ununiformed deviation from the original GB to the migrated GB.

All crack tips prepared from the three austenitic alloys in Table 2 were analysed by the techniques presented above. The lengths of IOZ and Cr-Fe depleted/Ni enriched zone ahead of the crack tips and maximum DIGM-induced GB deviations were obtained. To account for the statistical variations in the results obtained by the high-resolution analytical TEM (ATEM), all parameters measured from each material under each temperature are averaged. The results are summarized in Table 3. It should be noted that although the crack tips used in this study are potentially active, the different CGRs in different alloys may still result in different exposure times for these crack tips, which will, to some extent, affect the DIGM and intergranular oxidation. However, with the approach used in the present study, this kind of effect should have been minimized.

3.3 Identification of elemental diffusion in the DIGM zone

Although the formation of DIGM zone ahead of the SCC crack tips is due to elemental diffusion [2-8], the detailed diffusion paths of different alloying elements during the process need further investigation. Compared with the sizes of the DIGM zone formed in Fe-16Cr-11Ni alloy and Fe-16Cr-75Ni alloy, the size of the DIGM zone formed in Fe-16Cr-60Ni alloy tested at 360 °C is much larger. In addition, as shown in Fig. 5c, the overlap between the DIGM zone and the surrounding features, such as the IOZ and the metal matrix, is relatively small, enabling a large pure DIGM zone, optimum for elemental diffusion analysis. Hence, the DIGM zone formed in Fe-16Cr-60Ni alloy tested at 360 °C (Fig. 5) was selected for the examination of elemental diffusion during the occurrence of DIGM.

TKD was conducted to analyse the metallographic orientation of the two grains adjacent to the GB, as shown in Fig. 8. The inverse pole figure (IPF) map confirms the occurrence of DIGM, showing the migration from the bottom grain into the upper grain (Fig. 8b). The positions of the original and migrated GBs are marked by the red and blue dashed lines in the pattern quality map, respectively (Fig. 8a). TEM imaging was also conducted to confirm the occurrence of DIGM. As shown in Fig. 9a, the positions of the original and migrated GBs are observable, which are marked by the red and blue dashed lines, respectively. Fresnel contrast TEM imaging was conducted to reveal the nanoporosity of the intergranular oxide ahead of the SCC crack tip. The results show that the IOZ is nanoporous, with many nanochannels and nanopores observed (Figs. 9b, c, and d). Furthermore, SAED reveals that the oxides in the IOZ are mainly composed of Cr_2O_3 and Cr-Fe-Ni spinel (examined region is marked by the yellow dashed line in Fig. 9a).

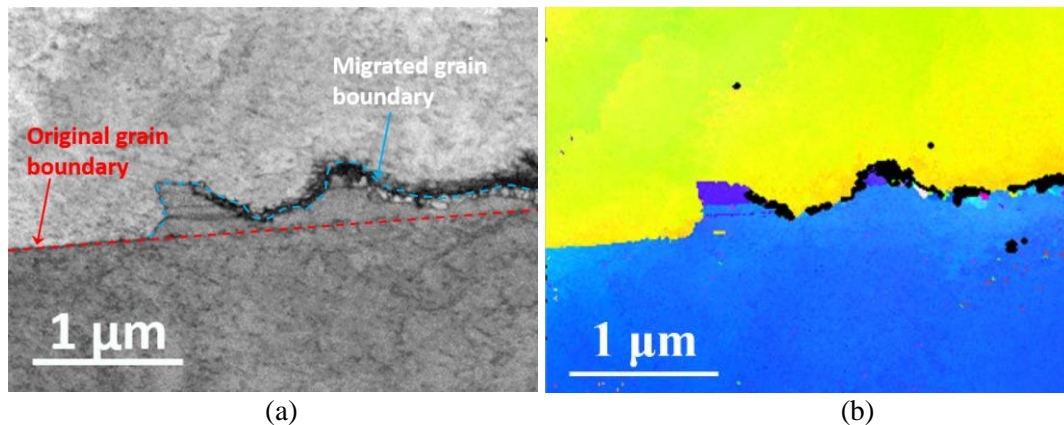


Fig. 8. TKD maps showing the DIGM around the crack tip of Alloy 60Ni tested at 360 °C: (a) pattern quality map; (b) IPF map.

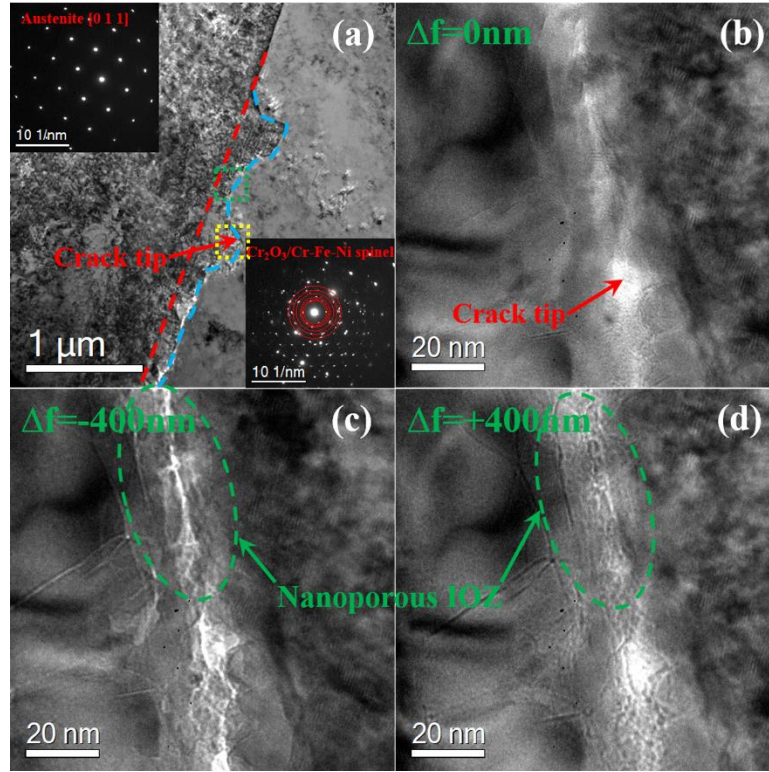


Fig. 9. (a) DFTEM image showing DIGM around the crack tip of Alloy 60Ni tested at 360 °C; Fresnel contrast TEM (b) in-focused, (c) under-focused, and (d) over-focused images showing the nanoporous IOZ.

To reveal the diffusion paths of the alloying elements during the process of DIGM, three EELS signal intensity line-scans were conducted across the DIGM zone (perpendicular to the original GB). As shown in Fig. 10a, the distances between the line-scan positions and the crack tip are different, decreasing from the line-scan 1 to the line-scan 2 and the line-scan 3. Compared with the positions of the line-scans 2 and 3, the position of line-scan 1 is furthest away from the crack tip, suggesting that DIGM occurred at the position of line-scan 1 has experienced less time than that occurred at the positions of line-scans 2 and 3. As shown in Fig. 10b, three composition gradients are observed across the DIGM zone. The composition gradients 1 and 3 are believed to be caused by the overlap between the DIGM zone and surrounding metal matrix. However, the composition gradient 2 can be assumed to be the real composition gradient in the DIGM zone since the composition gradient is not observed in the region free of DIGM. In the DIGM zone, it is seen that the signal intensities of Cr and Fe increase from the migrated GB towards the original GB while Ni exhibits an opposite trend (not including the overlap region). The overall signal intensities of Cr and Fe in the DIGM zone are lower than that in the surrounding metal matrix, suggesting that Cr and Fe have diffused out from the DIGM zone to other regions. Since the overall signal intensity of Ni is greater in the DIGM zone than that in the surrounding metal matrix, it suggests that Ni has diffused into the DIGM zone from other regions. Composition gradient is also observed in line-scan 2, as shown in Fig. 10c. The composition gradient 4 is believed to be the real composition gradient in the DIGM zone and the gradient 5 is believed to be due to overlap. The variation of Ni and Cr signal intensities in the line-scan 2 is similar to that observed in the line-scan 1 while the signal intensity of Fe is nearly uniform and no gradient is observed. The composition gradient 6 is believed to be the real composition gradient in the DIGM zone and the composition gradient 7 is believed to be due to overlap (Fig. 10d). The signal intensities of Fe, Cr, and Ni are all nearly uniform in the DIGM zone.

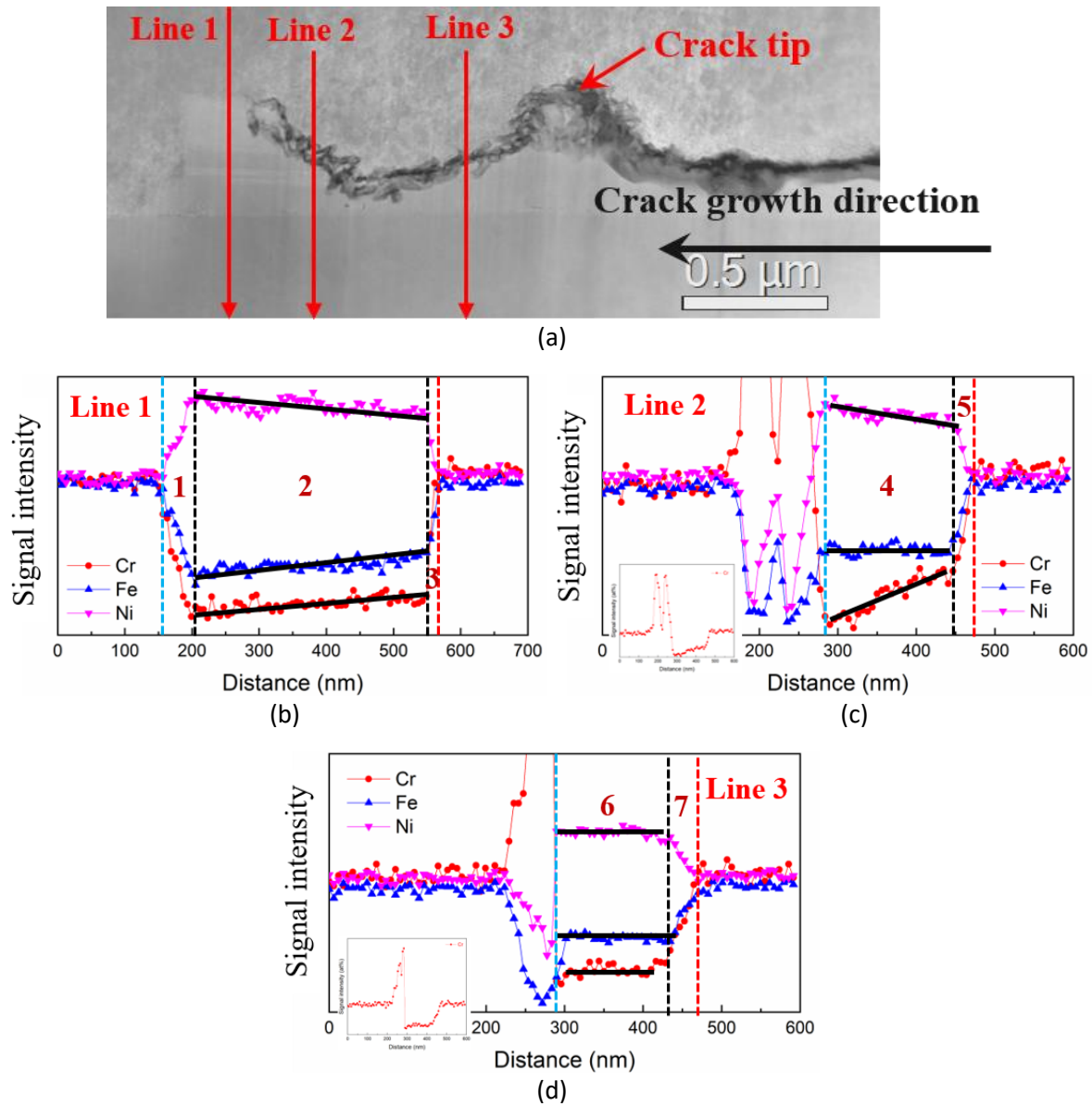


Fig. 10. (a) HAADF image showing a representative SCC crack tip prepared from Fe-16Cr-60Ni alloy with indication of EELS line-scan positions; signal intensity line profiles obtained through EELS analysis performed at the positions of (b) Line 1, (c) Line 2, and (d) Line 3.

4. Discussion

All the SCC crack tip samples prepared from the three austenitic alloys after tested in PWR primary water at 320 and 360 °C are examined by high-resolution characterization. The formation of a Cr-rich IOZ, identified as the mixture of Cr_2O_3 and Cr-Fe-Ni spinel, is observed ahead of all the examined crack tips, always associated with the formation of a Cr-Fe depleted/Ni enriched zone aside and ahead of the IOZ. The IOZ is reported to be nanoporous [17, 34, 38, 50], which is also confirmed in the current study (Fig. 9). After more than 50 oxidized GBs were fractured by the micromechanical testing, none of the cracks was observed to propagate beyond the oxidized portion [26]. As a result, the formation of a nanoporous IOZ ahead of the SCC crack tips is supposed to be a precursor for SCC, and SCC crack propagation is believed to occur by successive cracking of the nanoporous IOZ [34, 38, 51]. The formation of a Cr-Fe depleted/Ni enriched zone aside and ahead of the IOZ has been widely reported to be due to DIGM [20-22, 34, 41, 43-48, 51], which is also confirmed in the current study (Figs. 4-6). The formation of a DIGM zone is reported to affect the intergranular oxidation [20-22, 34, 41, 43-48, 51]. A recent work conducted by Volpe et al. [20] has systematically studied the relationship between DIGM and intergranular oxidation in Alloy 600 after exposure to hydrogenated steam at 480 °C. However, to date, the relationship between the DIGM and SCC crack growth has been rarely studied, which requires a direct observation on the DIGM zone ahead of SCC crack tips. A detailed high-resolution characterization on a series of potentially active SCC crack tips has

been performed in this study. New insights into DIGM occurring ahead of SCC crack tips and the implications of the key observations reported in the previous section are discussed below.

4.1 Comparison between the DIGM occurring in diffusion couple and ahead of SCC crack tip

In 1938, the DIGM was firstly observed by Rhines and Montgomery [69] in the study of Zn-Cu diffusion couple. The following studies by the other researchers have clearly shown that GBs can migrate when solute atoms diffuse along them [2-8]. The process of DIGM is schematically shown in Fig. 11 [4]. If solute atoms diffuse into a GB from some source as in Fig. 11a under conditions where the lattice diffusion is difficult, the GB will migrate leaving behind a zone with increased alloy content, termed as alloyed zone, in its wake. If solute atoms diffuse out of a GB to some sink as in Fig. 11b the GB will also migrate leaving behind a zone with reduced alloy content, termed as de-alloyed zone, in its wake. Although the GB migration observed in the SCC community is also termed as DIGM, the differences between the DIGM observed in the SCC community and the DIGM observed in the diffusion couples also exist and are required to be emphasized.

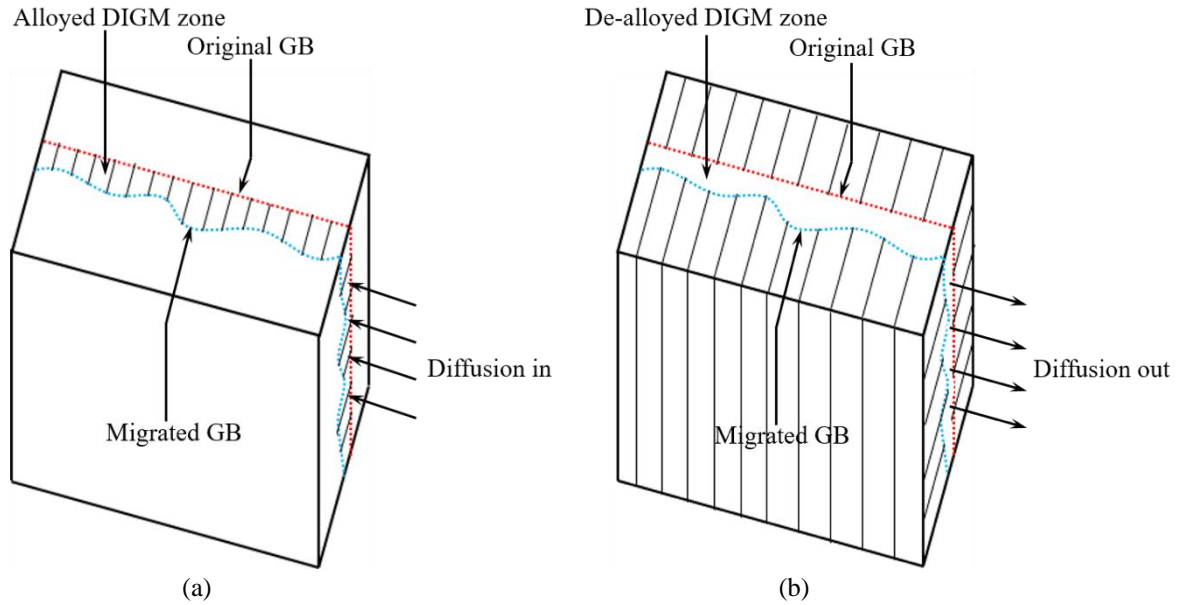


Fig. 11. Schematic images of DIGM in a region of a GB [4]. (a) Solute atoms are deposited during DIGM, and the GB migrates while leaving behind an alloyed zone. (b) Solute atoms are removed during DIGM, and the GB migrates while leaving behind a de-alloyed zone.

In the study of diffusion couples, DIGM has always been associated with solute atoms diffusion along GBs, and it is shown that DIGM cannot occur without diffusion [4]. As a result, the driving force for the DIGM occurred in the diffusion couple is believed to be chemical composition variation between the couple [5, 6]. Burke et al. [46] and Nguejio et al. [51] only observed DIGM in the simulated PWR primary water where preferential oxidation of Cr and Fe occurred while no DIGM was observed in the same high-temperature vacuum environment, free of oxidation. As a result, the preferential oxidation of Cr and Fe is believed to be indispensable in the DIGM observed in the SCC community [46, 51]. In addition, since the IOZ is always associated with the DIGM, there could be some relationship between the IOZ and DIGM. According to the results observed in the present study, the lateral migration of the GB terminates once newly migrated GB is preferentially oxidized, suggesting that the PIO can shield the further lateral migration of the GB. Similar results are also reported by the previous researchers [20-22, 34, 41, 43-48, 51]. Although the lateral migration of the GB can be terminated by the PIO, the DIGM can still develop in depth along the original GB since the DIGM zone is always observed ahead of the PIO zone.

As mentioned above, the DIGM occurred in the diffusion couple is driven by the chemical interdiffusion between the couple. Although the DIGM occurred in the oxidized GBs [20, 21, 43-48, 51] and ahead of the SCC crack tips [22, 34, 41] is believed to be due to elemental diffusion of less noble elements, which are Cr and Fe in the case of austenitic alloys in primary PWR conditions, the detailed description of the process has been scarcely reported. The high-resolution EELS chemical composition line-scanning (Fig. 10) conducted in the present study enables a detailed analysis on this topic. The results show that the overall net contents of Cr and Fe in the DIGM zone is lower than that in the metal matrix (Figs. 10b-d). The decrease of Cr and Fe in the DIGM zone should have been consumed by the PIO at the migrated GB. As shown in Fig. 10b, the composition gradients of Cr and Fe decreasing from the original GB towards the migrated GB are observed, which is consistent with a lateral GB migration direction. As a result, it is sensible to attribute the DIGM to the outward

diffusion of less-noble elements (Cr and Fe). It is surprising that the Ni content in this direction is also not constant and an inverse concentration gradient (compared to Cr and Fe) is observed (Fig. 10b). Since the overall net content of Ni in the DIGM zone is higher than that in the metal matrix and Ni is depleted in the IOZ, the enriched Ni in this zone is believed to be originated from the IOZ. The observation of the Ni concentration gradient in the DIGM zone suggests that the DIGM is not just driven by the diffusion of less-noble elements (Cr and Fe) but also by the diffusion of Ni. The variation of chemical composition gradients in Figs. 10b-d suggests that although the PIO of the migrated GB can terminate the further lateral migration, the lateral elemental diffusion in the DIGM zone cannot be terminated immediately. Ni, Cr, and Fe will keep diffusing laterally until the concentration gradients disappear. Consequently, according to the results obtained above, the DIGM occurring ahead of the SCC crack tips is believed to be driven by elemental diffusion, including both less-noble and more-noble elements. The elemental diffusion processes during the DIGM have been schematically shown in Fig. 12.

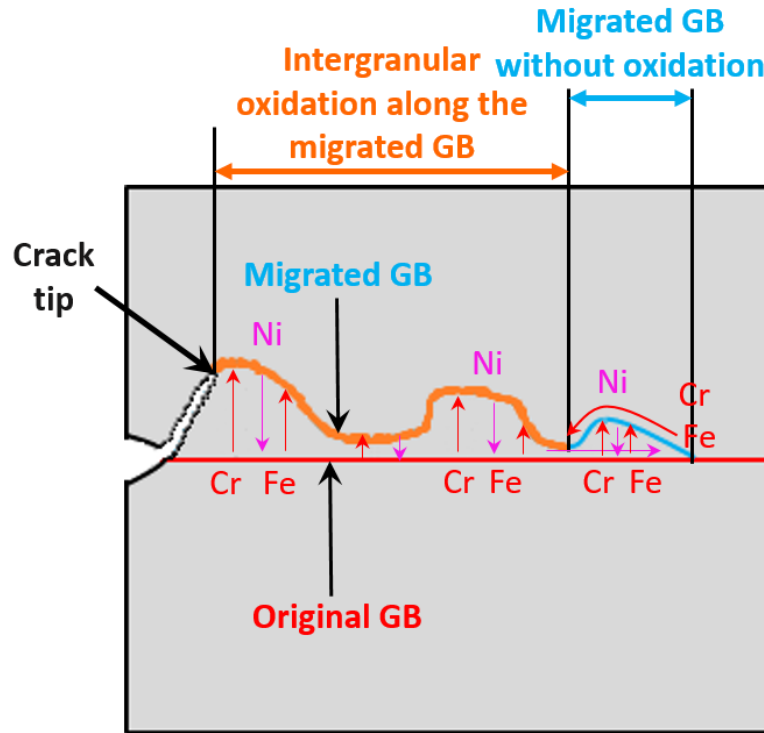


Fig. 12. Schematic image showing the diffusion of Fe, Cr, and Ni ahead of SCC crack tip during the process of PIO and DIGM.

Although the DIGM observed ahead of the SCC crack tips has been proven to be activated by the elemental diffusion in the present study, no diffusion couple exists ahead of the SCC crack tips driving the elemental diffusion. Instead, the elemental diffusion ahead of the SCC crack tips is driven by the preferential oxidation of Cr and Fe along the migrated GBs but not by the variation of chemical composition between the couple. The IOZ ahead of the SCC crack tips formed by the preferential oxidation of Cr and Fe works as a sink to store the outward diffusion of Cr and Fe from the DIGM zone and drives the continuous outward diffusion of Cr and Fe until reaches a balance state. Although the diffusion of less-noble elements (Cr and Fe) during the process of DIGM has been widely acknowledged [20-22, 34, 41, 43-48, 51], the diffusion of noble elements (Ni) has not received enough attention. As shown in the oxidized crack flanks of Fe-16Cr-11Ni alloy (Fig. 1), Ni segregation is observed under the thin Cr-rich oxide layer on the crack flanks. Similar results are also reported by Shen et al. [55, 56] and have been systematically studied. The authors found that the Ni segregation is the results of selective oxidation less-noble elements (Cr and Fe) and expulsion of noble elements (Ni) from the internal oxide precipitates into the surrounding matrix when the materials is exposed to the hydrogenated PWR primary water. Since the water chemistry used in the present study is the same with that in [55, 56], as a result, the Ni segregation observed in the crack flanks is also believed to be due to the selective oxidation of less-noble elements (Cr and Fe) and expulsion of noble elements (Ni). As mentioned above, Cr and Fe diffuse out from the DIGM zone and are preferential oxidized at the migrated GB, leaving a large number of vacancies in the DIGM zone. The unoxidized Ni in the IOZ is expelled and diffuses into the DIGM zone, leading to the formation of a reverse Ni concentration gradient in the DIGM zone compared with Cr and Fe. The expulsion of Ni was also observed on the surface of alloy 600 after exposure to hydrogenated steam by the other research groups [44, 67], which was also supposed to be due to the selective oxidation of less-noble elements (Cr and Fe) and expulsion of noble elements (Ni).

It is necessary to point out that the DIGM observed ahead of the SCC crack tips always occurs in one of the adjacent two grains, which is different from that observed in the diffusion couples where new GBs migrated into both of the adjacent two grains. This difference is supposed to be due to the differences in deformation in the adjacent two grains during the prior 20% CW, which has been proven by Shen et al. [38] in a 20% CW Alloy 600 via EBSD analysis. Since the DIGM is mainly controlled by elemental diffusion, the grain within higher dislocation density will facilitate the elemental diffusion and might result in a preferential migration in this grain. In addition, the external stress loaded at the specimen during the SCC testing might also contribute to this preferential DIGM in one of the adjacent two grains when the Schmid factors of the adjacent two grains are different. Different Schmid factors will lead to different extents of deformation under the external stress in the adjacent two grains. The GB could preferentially migrate into the grain suffered greater extent of deformation.

4.2 Effects of temperature and alloy composition on DIGM

DIGM is observed ahead of all the SCC crack tips prepared from the three austenitic alloys, suggesting that it occurs before the SCC crack growth. However, the extents of DIGM in different alloys and under different temperatures are different (Table 3), which indicates that the DIGM could be affected by the alloy composition and temperature. In the present study, two parameters are measured and used to quantify the extent of DIGM in different alloys and under different temperatures: one is the length of DIGM zone along the original GB and the other one is the width of DIGM zone caused by GB lateral deviation. Since the deviation induced by DIGM is not uniform, the maximum deviation is used to represent the width of the DIGM zone (Fig. 7).

4.2.1 Temperature

It is seen that both the length and width of the DIGM zone in the three alloys increase with the temperature. However, the acceleration effects introduced by the temperature in the three alloys are different. Compared with Fe-16Cr-11Ni alloy and Fe-16Cr-75Ni alloy, the DIGM in Fe-16Cr-60Ni appears to be more sensitive to temperature since both the length and width of the DIGM zone in this alloy are more than three times larger at 360 °C than that at 320 °C. In the study of Ag-Cu diffusion couple, the DIGM was also observed to be enhanced by the temperature [3]. The authors attributed the enhanced DIGM to the accelerated elemental diffusion at higher temperature and it is the proposed explanation for the observations in this study. As to the different temperature-acceleration effects in the different alloys, two possible explanations can be proposed. The first one might be the different temperature dependence of PIO susceptibility in the three different alloys. According to the results presented above, the formation of DIGM is driven by the PIO-induced elemental diffusion. The different extent of PIO will inevitably cause different extent of DIGM. The second one might be the different temperature dependence of mechanical deformation around the SCC crack tips of the three different alloys. In the study of dislocation accumulation around the SCC crack tips under an external loading in two austenitic alloys (316 stainless steel and Alloy 600) [19, 34], the authors found that the extent of dislocation accumulated around the SCC crack tip of 316 stainless steel decreases with the increase of temperature, while Alloy 600 is nearly independent with the temperature. Although the dislocation density around the SCC crack tips of the three different alloys has not been measured, the different temperature dependence of mechanical deformation in the three different alloys can be expected according to the results reported in [19, 34]. Since the dislocation density in the alloys has been widely reported to affect the elemental diffusion [70, 71], the different dislocation density around the SCC crack tips of the three different alloys will also have different extent of effects on the DIGM.

It is worth noting that although dissolved hydrogen contents at 320 and 360 °C were set as 30 cc/kg, the temperature has been revealed to affect the position of the Ni/NiO equilibrium boundary [72, 73]. Hence, the actual electrochemical potentials at 320 and 360 °C were different, which can affect the oxidation and may also contribute to the different extent of DIGM observed at different temperatures. However, according to the work conducted by Volpe et al. [20], the relatively small difference of temperature (320 and 360 °C) could only result in a small difference at electrochemical potential. In addition, no changes in oxide composition were observed in the crack tip region. Compared with the differences of DIGM caused by the electrochemical potential, the differences caused by the temperature are believed to be the dominant ones.

4.2.2 Alloy composition

Although the DIGM has been extensively studied in the SCC community [20-22, 34, 41, 43-48, 51], to date nearly all the studies focus on a single alloy (Alloy 600 or Alloy 690). Hence, the effect of alloy composition on the DIGM has been scarcely reported. In the present study, the DIGM in the three alloys within different alloy composition is directly compared. It is seen that both the length and width of the DIGM zone are affected by alloy composition. Compared with the DIGM at 320 °C, the effect of alloy composition on the DIGM is much larger at 360 °C. According to the results shown in Table

3 and the results discussed above, both the PIO and DIGM are accelerated at higher temperature. As a result, the enhanced effect of alloy composition on the DIGM at 360 °C could be because the difference caused by the alloy composition is enlarged at higher temperature.

The different effects of alloy composition on the DIGM at 320 and 360 °C suggests that the temperature and alloy composition can affect the DIGM simultaneously. The effects of temperature on the DIGM has been discussed above. If the temperature is fixed, the DIGM length and width still vary with the content of Ni in the alloys. This variation is believed to be caused by the alloy composition. As mentioned above, the formation of DIGM ahead of the SCC crack tips is the result of the PIO driving the diffusion of Cr, Fe, and Ni. As a result, the factors that affect PIO may also affect the DIGM. Cr content is widely known to play a critical role in affecting the oxidation of austenitic alloys [34, 74]. Although the Cr content in the three alloys remains the same, the contents of Fe and Ni are different. In a recent work conducted by Ru et al. [75], the Fe content in the Ni-33Cr-xFe austenitic alloys was also reported to affect the oxidation of the alloys. The results show that the corrosion resistance of the surface oxide scale decreases with the increase of Fe content when the Cr remains constant. In the present study, since all the SCC crack tips were prepared from the deepest region of the SCC cracks and are supposed to be active at the end of the SCC testing, they are supposed to be exposed to the PWR primary water for similar amount of time. Hence the lengths of the IOZ ahead of the SCC crack tips are used to quantify the PIO rates ahead of SCC crack tips. Table 3 shows that Fe-16Cr-60Ni alloy exhibits a much faster intergranular oxidation rate than the other two alloys, which is different from the results reported in [75]. This difference might be due to the different effects of Fe content on the intragranular [75] and intergranular oxidation. Although the detailed mechanisms controlling the difference is still unclear, the results observed in the present study indicate that, except from Cr, the contents of Fe and Ni in the alloys should also be considered in the design of intergranular oxidation-resistant alloys. In addition, in the study of DIGM in Alloy 600 under the hydrogenated steam containing different content of dissolved hydrogen, Volpe et al. [20] found that the GBs suffered minor PIO tend to have a short and wide DIGM zone while the GBs suffered significant PIO tend to have a long and narrow DIGM zone. Similar results are also reported by Shen et al. [22], and the authors assumed that a faster PIO can lead to a smaller DIGM width and a larger DIGM length and vice versa. The alloy composition could first affect the DIGM through affecting the PIO, and the result of PIO can then also affect the following DIGM.

Compared with the length and width of the DIGM zone, the length of the IOZ ahead of the SCC crack tips in the different alloys and at each temperature generally exhibit a similar trend with the DIGM length and width. For example, Fe-16Cr-60Ni alloy has faster PIO rates than the other two alloys and both the lengths and widths of their DIGM zones are larger than the other two alloys. These results show that a faster PIO may not necessarily lead to a smaller DIGM width and a larger DIGM length, which contradicts to the conclusions obtained in the study of DIGM in a single alloy [20, 22]. As a result, no simple conclusions can be made about how much the temperature and alloy composition can affect the DIGM. The DIGM occurring ahead of the SCC crack tips is the competing result of elemental lateral and in-depth diffusion and PIO, with the three processes interconnected. Consequently, both the temperature and alloy composition are believed to affect the DIGM but have different weights across the three austenitic alloys in the present study.

4.3 Potential correlation between the DIGM and SCC crack growth

Although various SCC models have been proposed [27-32], the PIO model appears to describe the degradation of austenitic alloys in PWR primary water most realistically [20, 33-39]. A recent work [26] shows that all the oxidized GBs (more than 50) were fractured under the micro-mechanical testing while none of the cracks advanced beyond the oxidized portion. Hence, it is proposed that the intergranular oxidation is prerequisite for SCC crack growth and the CGR was believed to be proportional to the intergranular oxidation rate. In other words, a faster intergranular oxidation rate would result in a faster CGR and vice versa. As mentioned above, the length of the IOZ ahead of the SCC crack tips are used to quantify the intergranular oxidation rate if they are assumed to be exposed to the PWR primary water for the same amount of time. As shown in Tables 2 and 3, the CGRs of Fe-16Cr-11Ni alloy and Fe-16Cr-75Ni alloy correlate well with the IOZ lengths at 320 and 360 °C, which appears to support the proportional relationship between the intergranular oxidation rate (IOZ length) and CGR. However, as to Fe-16Cr-60Ni alloy, the IOZ length at 360 °C is larger than that at 320 °C while the CGR shows an opposite trend. It suggests that a faster intergranular oxidation rate may not necessarily lead to a faster CGR. As a result, the CGR does not depend entirely on the intergranular oxidation rate and other factors also contribute.

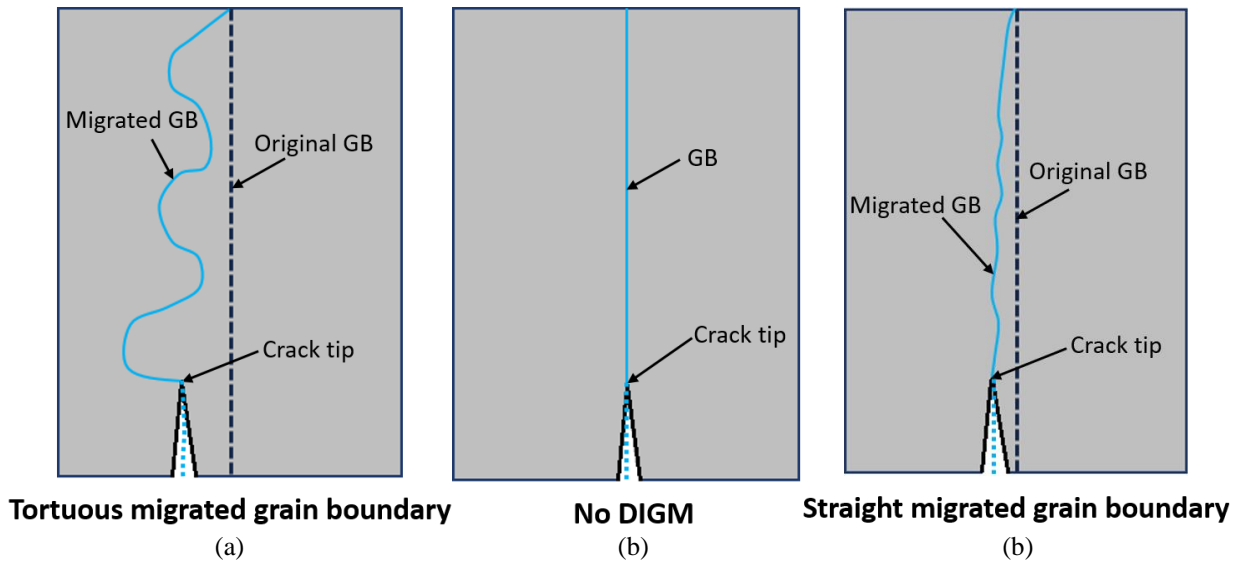


Fig. 13. Schematic images showing the SCC crack growth along different types of GBs: (a) a tortuous migrated GB; (b) a GB without DIGM; (c) a straight migrated GB.

To understand the relationship between the intergranular oxidation rate and CGR in Fe-16Cr-60Ni alloy, further attention has been paid on the morphology of the DIGM zone formed ahead of the SCC crack tips. Although the DIGM zone is observed ahead of all the SCC crack tips, the shapes of the migrated GBs are different. The migrated GBs can be qualitatively divided into two different groups: one is a tortuous migrated GB (Group 1) and the other one is a (relatively) straight migrated GB (Group 2), as shown in Figs. 13a and c, respectively. As shown in Fig. 2a, the migrated GB in Fe-16Cr-60Ni alloy at 360 °C belongs to Group 1, while the migrated GB at 320 °C belongs to Group 2. Compared with the GB without DIGM (Fig. 13b), the SCC crack propagation along the tortuous migrated GB (Group 1) will change the effective stress state at the crack tip since the propagation will be diverted to a path no longer perpendicular to the applied load, which will then retard the SCC crack growth. As to the straight migrated GB (Group 2), the crack would propagate following a direction almost parallel to the original G (with minimal changes to the effective stress), leading to a minor retardation effect on the SCC crack growth. In addition, the crack path is longer for tortuous migrated GBs when compared with straight ones. Consequently, the abnormal relationship between the intergranular oxidation rate and CGR in Fe-16Cr-60Ni alloy at 320 and 360 °C can be attributed to the retardation effects caused by the formation of tortuous migrated GBs at 360 °C (Group 1). For the migrated GBs in Fe-16Cr-11Ni alloy and Fe-16Cr-75Ni alloy, they all belong to Group 1 and the retardation effect caused by the relatively straight GB is very limited, resulting in a well correlation between the intergranular oxidation rate and CGR.

It is reported that the elemental diffusion along “active” migrating GBs is faster than that along stationary GBs [5, 76]. As a result, the DIGM is supposed to accelerate the O and Cr diffusivities along the GBs, resulting a faster intergranular oxidation rate [20]. As shown in Table 3, the variation of the lengths of the IOZ in the three alloys show a similar trend with the variation of the lengths and widths of the DIGM zone in these alloys, which appears to support the hypothesis proposed in [20]. The diffusion of minor alloying elements Al and Ti is also believed to be enhanced during the DIGM since they are significantly enriched along the migrated GBs [20, 44, 48]. Since these elements are readily oxidized to Al_2O_3 and TiO_2 , the intergranular diffusion of oxygen is supposed to be enhanced along the interfaces between matrix and oxide (Al_2O_3 and TiO_2) once these minor alloying elements are oxidized [20, 44, 48, 77]. No Al and Ti are detected in the alloys used this study. Hence their potential effects on the oxidation of the migrated GBs cannot be evaluated by the data obtained in the present study.

5. Conclusions

It is proposed that DIGM ahead of SCC crack tips plays a critical role in SCC crack propagation. Potentially active SCC crack tips prepared from three different austenitic alloys after tested in simulated PWR primary water at 320 and 360 °C were analysed to understand the process of DIGM ahead of the SCC crack tips and its role on SCC crack propagation. By applying a range of complementary analytical microscopy techniques, the following conclusions can be drawn:

1. DIGM is observed ahead of all the SCC crack tips and the crack propagation develops along the migrated GB.

2. The formation of DIGM ahead of SCC crack tips has been compared with that occurred in the diffusion couple. The DIGM occurred ahead of SCC crack tips is the result of Cr, Fe, and Ni diffusion driven by PIO, which is different from that in the diffusion couple, in which the DIGM occurs due to the prior existence of chemical composition gradient between the couple.

3. The DIGM length and width are the result of competing elemental lateral and in-depth diffusion and PIO. Although the PIO shields the further lateral migration of GBs, the in-depth migration can further develop.

4. Faster intergranular oxidation may not necessarily lead to faster CGR because the crack path along a migrated GB may be longer due to its tortuous nature.

Declaration of Competing Interest

We declare that we do not have any commercial or associative interest that represents a conflict of interest in connection with the work submitted.

Data availability

The raw unpublished supporting data are available upon request.

CRedit authorship contribution statement

Zhao Shen: Conceptualization, Methodology, Investigation, Writing - original draft. **Koji Arioka:** Conceptualization, Methodology, Investigation, Writing - original draft. **Sergio Lozano-Perez:** Conceptualization, Data curation, Formal analysis, Funding acquisition, Investigation, Project administration, Supervision, Writing - review & editing.

Acknowledgements

The authors would like to thank INSS (Japan) for providing the samples used in this study. Zhao Shen is grateful to China Scholarship Council (CSC) for providing financial support to his PhD studentship. The EPSRC (EP/K040375/1, EP/N010868/1 and EP/R009392/1) grants are also acknowledged for funding this research.

References

- [1] D.G. Brandon, The structure of high-angle grain boundaries, *Acta Metall.* 14(1966) 1479-1484.
- [2] A.H. King, Diffusion induced grain boundary migration, *Int. Mater. Rev.* 32(1987) 173-189.
- [3] Z. Guan, G. Liu, J. Du, Characterization of diffusion induced grain boundary migration in the Ag/Cu system. *Acta Metall.* 41(1993) 1293-1300.
- [4] R.W. Balluffi, J.W. Cahn, Mechanism for diffusion induced grain boundary migration, *Acta Metall.* 29(1981) 493-500.
- [5] M. Hillert, G.R. Purdy, Chemically induced grain boundary migration, *Acta Metall.* 26(1978) 333-340.
- [6] M. Hillert, On the driving force for diffusion induced grain boundary migration, *Scripta Metall.* 17(1983) 237-240.
- [7] I. Toda-Caraballo, P.D. Bristowe, C. Capdevila, A molecular dynamics study of grain boundary free energies, migration mechanisms and mobilities in a bcc Fe-20Cr alloy, *Acta Mater.* 60(2012) 1116-1128.
- [8] A.T. Wicaksono, C.W. Sinclair, M. Militzer, An atomistic study of the correlation between the migration of planar and curved grain boundaries, *Comp. Mater. Sci.* 117(2016) 397-405.
- [9] D. Caillard, F. Momprou, M. Legros, Grain-boundary shear-migration coupling. II. Geometrical model for general boundaries, *Acta Mater.* 57(2009) 2390-2402.
- [10] C.H. Li, E.H. Edwards, J. Washburn, E.R. Parker, Stress-induced movement of crystal boundaries, *Acta Metall.* 1(1953) 223-229.
- [11] T. Gorkaya, D.A. Molodov, G. Gottstein, Stress-driven migration of symmetrical $\langle 1\ 0\ 0 \rangle$ tilt grain boundaries in Al bicrystals, *Acta Mater.* 57(2009) 5396-5405.
- [12] T.J. Rupert, D.S. Gianola, Y. Gan, K.J. Hemker, Experimental observations of stress-driven grain boundary migration, *Science* 326(2009) 1686-1690.
- [13] S. Lozano-Perez, J. Dohr, M. Meisnar, K. Kruska, SCC in PWRs: learning from a bottom-up approach, *Metall. Mater. Trans. E* 1(2014) 194-210.
- [14] T. Shoji, Z. Lu, Q. Peng, *Stress Corrosion Cracking: Theory and Practice* (Woodhead, Cambridge, 2011), pp. 245–272.
- [15] W. Bamford, J. Hall, Cracking of alloy 600 nozzles and welds in PWRs: review of cracking events and repair service experience. In *Proceedings of the 12th International Conference on Environmental Degradation of Materials in Nuclear Power System-Water Reactors*, Salt Lake City, UT, 2005 (p. 959).
- [16] P.L. Andresen, M.M. Morra, Stress corrosion cracking of stainless steels and nickel alloys in high-temperature water, *Corrosion* 64 (2008) 15-29.

- [17] L.E. Thomas, S.M. Bruemmer, High-resolution characterization of intergranular attack and stress corrosion cracking of Alloy 600 in high-temperature primary water, *Corrosion* 56(2000) 572-587.
- [18] R.P. Matthews, R.D. Knusten, J.E. Westraadt, T. Couvant, Intergranular oxidation of 316L stainless steel in the PWR primary water environment, *Corros. Sci.* 125(2017) 175-183.
- [19] M. Meisnar, A. Vilalta-Clemente, M. Moody, K. Arioka, S. Lozano-Perez, A mechanistic study of the temperature dependence of the stress corrosion crack growth rate in SUS316 stainless steels exposed to PWR primary water, *Acta Mater.* 114 (2016) 15-24.
- [20] L. Volpe, M. G. Burke, F. Scenini. Understanding the Role of Diffusion Induced Grain Boundary Migration on the Preferential Intergranular Oxidation Behaviour of Alloy 600 via Advanced Microstructural Characterization. *Acta Mater.* 175(2019) 238-249.
- [21] M. Sennour, P. Laghoutaris, C. Guerre, R. Molins, Advanced TEM characterization of stress corrosion cracking of Alloy 600 in pressurized water reactor primary water environment, *J. Nucl. Mater.* 393(2009) 254-266.
- [22] Z. Shen, P. Karamched, K. Arioka, S. Lozano-Perez, Observation and quantification of the diffusion-induced grain boundary migration ahead of SCC crack tips. *Corros. Sci.* 147(2019) 163-168.
- [23] H. Dugdale, D.E. Armstrong, E. Tarleton, S.G. Roberts, S. Lozano-Perez, How oxidized grain boundaries fail, *Acta Mater.* 61(2013) 4707-4713.
- [24] Y. Han, J. Mei, Q. Peng, E.H. Han, W. Ke, Effect of electropolishing on corrosion of nuclear grade 316L stainless steel in deaerated high temperature water, *Corros. Sci.* 112(2016) 625-634.
- [25] T. Terachi, K. Fujii, K. Arioka, Microstructural characterization of SCC crack tip and oxide film for SUS 316 stainless steel in simulated PWR primary water at 320 C, *J. Nucl. Sci. Technol.* 42(2005) 225-232.
- [26] J. Dohr, D.E. Armstrong, E. Tarleton, T. Couvant, S. Lozano-Perez, The influence of surface oxides on the mechanical response of oxidized grain boundaries. *Thin Solid Films*, 632(2017) 17-22.
- [27] E.M. Gutman, An inconsistency in “film rupture model” of stress corrosion cracking, *Corros. Sci.* 49(2007) 2289-2302.
- [28] H.L. Logan, Film-rupture mechanism of stress corrosion, *J. Res. Natl. Bur. Stand.* 48(1952) 99-105.
- [29] S.P. Lynch, Environmentally assisted cracking: overview of evidence for an adsorption-induced localised-slip process, *Acta Metall.* 36(1988) 2639-2661.
- [30] C.D. Beachem, A new model for hydrogen-assisted cracking (hydrogen “embrittlement”), *Metall. Mater. Trans. B* 3(1972) 441-455.
- [31] K. Arioka, 2014 WR Whitney Award Lecture: Change in Bonding Strength at Grain Boundaries Before Long-Term SCC Initiation, *Corrosion* 71(2014) 403-419.
- [32] K. Arioka, T. Yamada, T. Miyamoto, T. Terachi, Dependence of stress corrosion cracking of alloy 690 on temperature, cold work, and carbide precipitation—role of diffusion of vacancies at crack tips, *Corrosion* 67(2011) 035006-1.
- [33] P.M. Scott, M. Le Calvar. “Some possible mechanisms of intergranular stress corrosion cracking of alloy 600 in PWR primary water”. In *Proceedings of the sixth international symposium on environmental degradation of materials in nuclear power systems-water reactors*, (TMS, 1993), pp. 657-665.
- [34] Z. Shen, M. Meisnar, K. Arioka, S. Lozano-Perez, Mechanistic understanding of the temperature dependence of crack growth rate in alloy 600 and 316 stainless steel through high-resolution characterization, *Acta Mater.* 165(2019) 73-86.
- [35] G. Bertali, F. Scenini, M.G. Burke, N. Huin, The effect of temperature on the preferential intergranular oxidation susceptibility of alloy 600, *Metall. Mater. Trans. A*, 49A (2018) 1879-1894.
- [36] B.M. Capell, G.S. Was, Selective internal oxidation as a mechanism for intergranular stress corrosion cracking of Ni-Cr-Fe alloys, *Metall. Mater. Trans. A* 38(2007) 1244-1259.
- [37] Y.S. Lim, H.P. Kim, S.S. Hwang. Microstructural characterization on intergranular stress corrosion cracking of Alloy 600 in PWR primary water environment, *J. Nucl. Mater.* 440(2013) 46-54.
- [38] Z. Shen, K. Arioka, S. Lozano-Perez. A mechanistic study of SCC in Alloy 600 through high-resolution characterization, *Corros. Sci.* 132(2018) 244-259.
- [39] M.J. Olszta, D.K., Schreiber, M.B., Toloczko, S.M. Bruemmer, Alloy 690 Surface Nanostructures During Exposure to PWR Primary Water and Potential Influence on Stress Corrosion Cracking Initiation., In: *Proceedings of the 16th international symposium on environmental degradation of materials in nuclear power system—water reactors, minerals, metals and materials society/AIME* (2013).
- [40] M. Meisnar, M. Moody, S. Lozano-Perez, Atom probe tomography of stress corrosion crack tips in SUS316 stainless steels, *Corros. Sci.* 98(2015) 661-671.
- [41] W. Kuang, M. Song, G.S. Was, Insights into the stress corrosion cracking of solution annealed alloy 690 in simulated pressurized water reactor primary water under dynamic straining, *Acta Mater.* 151(2018) 321-333.
- [42] G. Economy, R.J. Jacko, F.W. Pement, IGSCC behavior of Alloy 600 steam generator tubing in water or steam tests above 360° C, *Corrosion* 43(1987) 727-734.
- [43] G. Bertali, F. Scenini, M. G. Burke, Advanced microstructural characterization of the intergranular oxidation of Alloy 600, *Corros. Sci.* 100 (2015) 474-483.
- [44] G. Bertali, F. Scenini, M. G. Burke, The effect of residual stress on the Preferential Intergranular Oxidation of Alloy 600, *Corros. Sci.* 111 (2016) 494-507.

- [45] G. Bertali, F. Scenini, M. G. Burke, The intergranular oxidation susceptibility of thermally-treated Alloy 600, *Corros. Sci.* 114(2017) 112-122.
- [46] M.G. Burke, G. Bertali, E. Prestat, F. Scenini, S.J. Haigh, The application of in situ analytical transmission electron microscopy to the study of preferential intergranular oxidation in alloy 600, *Ultramicroscopy* 176(2017) 46-51.
- [47] B. Langelier, S. Y. Persaud, A. Korinek, T. Casagrande, R. C. Newman, G. A. Botton, Effects of boundary migration and pinning particles on intergranular oxidation revealed by 2D and 3D analytical electron microscopy, *Acta Mater.* 131 (2017) 280-295.
- [48] S.Y. Persaud, B. Langelier, A. Korinek, S. Ramamurthy, G.A. Botton, R.C. Newman. Characterization of initial intergranular oxidation processes in alloy 600 at a sub-nanometer scale, *Corros. Sci.* 133(2018) 36-47.
- [49] D.K. Schreiber, M.J. Olszta, S.M. Bruemmer, Directly correlated transmission electron microscopy and atom probe tomography of grain boundary oxidation in a Ni–Al binary alloy exposed to high-temperature water, *Scripta Mater.* 69(2013) 509-512.
- [50] S.M. Bruemmer, M.J. Olszta, M.B. Toloczko, D.K. Schreiber, Grain boundary selective oxidation and intergranular stress corrosion crack growth of high-purity nickel binary alloys in high-temperature hydrogenated water. *Corros. Sci.* 131(2018) 310-323.
- [51] J. Nguejio, J. Crépin, C. Duhamel, F. Gaslain, C. Guerre, F. Jomard, M. Maisonneuve, Diffusion Processes as Possible Mechanisms for Cr Depletion at SCC Crack Tip. In *Proceedings of the 18th International Conference on Environmental Degradation of Materials in Nuclear Power Systems—Water Reactors*. Springer, Cham, 2019, pp. 337-357.
- [52] Z. Shen, J. Liu, K. Arioka, S. Lozano-Perez, On the role of intergranular carbides on improving the stress corrosion cracking resistance in a cold-worked alloy 600. *J. Nucl. Mater.* 514(2019) 50-55.
- [53] M. Meisnar, A. Vilalta-Clemente, A. Gholinia, M. Moody, A.J. Wilkinson, N. Huin, S. Lozano-Perez, Using transmission Kikuchi diffraction to study intergranular stress corrosion cracking in type 316 stainless steels, *Micron* 75(2015) 1-10.
- [54] W. Kuang, G.S. Was, A high-resolution characterization of the initiation of stress corrosion crack in Alloy 690 in simulated pressurized water reactor primary water. *Corros. Sci.*, 2019, In Press.
- [55] Z. Shen, D. Tweddle, M.T. Lapington, B. Jenkins, D. Du, L. Zhang, M.P. Moody, S. Lozano-Perez, Observation of internal oxidation in a 20% cold-worked Fe-17Cr-12Ni stainless steel through high-resolution characterization. *Scripta Mater.*, 173(2019) 144-148.
- [56] Z. Shen, D. Du, L. Zhang, S. Lozano-Perez, An insight into PWR primary water SCC mechanisms by comparing surface and crack oxidation, *Corros. Sci.* 148(2019) 213-227.
- [57] K. Arioka, T. Yamada, T. Miyamoto, M. Aoki, Intergranular Stress Corrosion Cracking Growth Behavior of Ni-Cr-Fe Alloys in Pressurized Water Reactor Primary Water, *Corrosion* 70(2014) 695-707.
- [58] S.M. Bruemmer, M. J. Olszta, M. B. Toloczko, L. E. Thomas. "High-resolution characterizations of grain boundary damage and stress corrosion cracks in cold-rolled alloy 690." In *Proceedings of the 15th International Conference on Environmental Degradation of Materials in Nuclear Power Systems—Water Reactors*, pp. 301-314. Springer, Cham, 2011.
- [59] W. Kuang, G.S. Was, The effects of grain boundary carbide density and strain rate on the stress corrosion cracking behavior of cold rolled Alloy 690, *Corros. Sci.* 97(2015) 107-114.
- [60] S.M. Bruemmer, M.J. Olszta, M.B. Toloczko, L.E. Thomas, Linking grain boundary microstructure to stress corrosion cracking of cold-rolled alloy 690 in pressurized water reactor primary water, *Corrosion* 69(2012) 953-963.
- [61] S. Lozano-Perez, K. Kruska, I. Iyengar, T. Terachi, T. Yamada, The role of cold work and applied stress on surface oxidation of 304 stainless steel, *Corros. Sci.* 56(2012) 78-85.
- [62] S. Lozano-Perez, A guide on FIB preparation of samples containing stress corrosion crack tips for TEM and atom-probe analysis, *Micron* 39(2008) 320-328.
- [63] K. Kruska, S. Lozano-Perez, D.W. Saxey, T. Terachi, T. Yamada, G.D.W. Smith, Nanoscale characterisation of grain boundary oxidation in cold-worked stainless steels, *Corros. Sci.* 63(2012) 225-233.
- [64] K. Chen, Z. Shen. A study on the surface and crack tip oxidation of alloy 600 through high-resolution characterization. *Corros. Sci.* 169(2020) 108616.
- [65] M. J. Olszta, D. K. Schreiber, M. B. Toloczko, S. M. Bruemmer. "Alloy 690 surface nanostructures during exposure to PWR primary water and potential influence on stress corrosion crack initiation." In *Proceedings of the 16th international symposium on environmental degradation of materials in nuclear power system—water reactors, minerals, metals and materials society/AIME*, 2013.
- [66] D.K. Schreiber, M.J. Olszta, S.M. Bruemmer, Grain boundary depletion and migration during selective oxidation of Cr in a Ni–5Cr binary alloy exposed to high-temperature hydrogenated water. *Scripta Mater.* 89(2014) 41-44.
- [67] B. Langelier, S.Y. Persaud, R.C. Newman, G.A. Botton, An atom probe tomography study of internal oxidation processes in Alloy 600. *Acta Mater.* 109(2016) 55-68.
- [68] S. Lozano-Perez, D.W. Saxey, T. Yamada, T. Terachi, Atom-probe tomography characterization of the oxidation of stainless steel. *Scripta Mater.* 62(2010) 855-858.
- [69] F.N. Rhines, and A.M. Montgomery, A new type of structure in the α -copper-zinc alloys. *Nature*, 141(1938) 413-413.
- [70] Z. Zhai, M.B. Toloczko, M.J. Olszta, S.M. Bruemmer, Stress corrosion crack initiation of alloy 600 in PWR primary water, *Corros. Sci.*, 123 (2017) 76-87.

- [71] Z. Shen, K. Chen, D. Tweddle, G. He, K. Arioka, S. Lozano-Perez, Characterization of the crack initiation and propagation in Alloy 600 with a cold-worked surface. *Corros. Sci.*, 152(2019) 82-92.
- [72] P.L. Andresen, J. Hickling, A. Ahluwalia, J. Wilson, Effects of hydrogen on stress corrosion crack growth rate of nickel alloys in high-temperature water, *Corrosion*, 64 (2008) 707-720.
- [73] S.A. Attanasio, D.S. Morton, Measurement of the Ni/NiO transition in Ni-Cr-Fe Alloys and updated data and correlation to quantify the effect of aqueous hydrogen on primary water SCC, *Proc. 11th Int. Symp. On Environmental Degradation of Materials in Nuclear Power Systems*, NRC, Rockville, MD (2003).
- [74] T. Terachi, T. Yamada, T. Miyamoto, K. Arioka, K. Fukuya. Corrosion behavior of stainless steels in simulated PWR primary water—effect of chromium content in alloys and dissolved hydrogen—. *J. Nucl. Sci. Technol.*, 45(2008) 975-984.
- [75] X. Ru, Z. Lu, J. Chen, G. Han, J. Zhang, P. Hu, X. Liang. Effects of iron content in Ni-Cr-xFe alloys and immersion time on the oxide films formed in a simulated PWR water environment. *J. Nucl. Mater.*, 497(2017) 37-53.
- [76] K. Smidoda, W. Gottschalk, H. Gleiter, Diffusion in Migrating Interfaces, *Acta Metall.* 26 (1978) 1833-1836.
- [77] R.C. Newman, F. Scenini, Another way to think about the critical oxide volume fraction for the internal-to-external oxidation transition?, *Corrosion* 64 (2008) 721–726.